

**Neurally-Controlled Ankle-Foot Prosthesis with  
Non-Backdrivable Transmission for Rock Climbing  
Augmentation**

by

Emily Rogers

S.B., Harvard University (2015)

Submitted to the Department of Mechanical Engineering  
in partial fulfillment of the requirements for the degree of

Master of Science

at the

MASSACHUSETTS INSTITUTE OF TECHNOLOGY

February 2019

© Massachusetts Institute of Technology 2019. All rights reserved.

**Signature redacted**

Author .....  
.....

/ Department of Mechanical Engineering

**Signature redacted** January 18, 2019

Certified by .....  
.....

Hugh Herr

Professor, Media Arts and Sciences

Thesis Supervisor

Certified by .....  
.....

Amos Winter

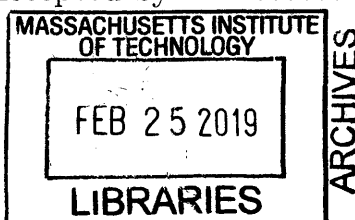
Associate Professor, Department of Mechanical Engineering

**Signature redacted** Thesis Reader

Accepted by .....  
.....

Nicolas Hadjiconstantinou

Chairman, Committee on Graduate Students





**Neurally-Controlled Ankle-Foot Prosthesis with  
Non-Backdrivable Transmission for Rock Climbing  
Augmentation**

by

Emily Rogers

Submitted to the Department of Mechanical Engineering  
on January 18, 2019, in partial fulfillment of the  
requirements for the degree of  
Master of Science

## **Abstract**

This thesis presents the design and evaluation of a neurally-controlled ankle-foot prosthesis optimized to enhance rock climbing ability in persons with transtibial amputation. The bionic rock climbing prosthesis restores biologic performance of the ankle-foot complex. The user volitionally controls the positions of both the prosthetic ankle and subtalar joints via input from electromyography surface electrodes worn on the residual limb. We hypothesize that a climbing specific robotic ankle-foot prosthesis will result in more biological emulation than a passive prosthesis. Specifically, we hypothesize that joint angles of the hip, knee, ankle, and subtalar of a person with transtibial amputation while rock climbing are more similar to the joint angles of a height-, weight-, and ability-matched control subject with intact limbs, compared to climbing with a passive prosthesis. To test the hypothesis, a powered, 2-degree-of-freedom, neurally controlled prosthesis is built that comprises a pair of non-backdrivable linear actuators providing 16 degrees of dorsiflexion, 18 degrees of plantar flexion, and 20 degrees each of inversion and eversion. The prosthesis operates at a bandwidth and range of motion matching biological free-space motion of the ankle and subtalar joint. Climbing performance is evaluated by measuring joint angles and muscle activity during rock climbing with the robotic prosthesis and a traditional passive prosthesis, and comparing the kinematic data to that of a subject with intact biological limbs. We find that the bionic prosthesis brings the ankle and subtalar joint angles of the subject to more similar angles than the control subjects with intact biological limbs, compared to a standard passive prosthesis. These results indicate that a lightweight, actuated, 2-degree-of-freedom neurally-controlled robotic ankle-foot prosthesis restores biological function to the user during an extremely technical sport.

Thesis Supervisor: Hugh Herr, Professor, Department of Media Arts and Sciences  
Reader: Amos Winter, Associate Professor, Department of Mechanical Engineering



## Acknowledgments

Thank you first and foremost to Professor Hugh Herr for the crazy ideas you come up with and the talent and knowledge to pull them off. Thank you for the opportunity to work on such an exciting project, and for all your support along the way. I also greatly appreciate the guidance and support of my thesis reader, Professor Amos Winter. I would like to thank the National Science Foundation for funding my graduate research through the Graduate Research Fellowship award.

Thanks to all my labmates in Biomechatronics, especially Matt Carney for your mechanical design expertise and mentorship, Seong Ho Yeon for the amazing design of the EMG system and all the fun hours spent at Brooklyn Boulders, Tyler Clites for your neuromuscular model contribution and EMG expertise, and Mike Nawrot for your machining and motion capture assistance. Thank you to everyone in Biomech for all the late nights, early mornings, coffee runs, debugging, and friendship.

Thanks to my friends and family for dragging me out of lab when I needed it, and for the long runs on the river. A special thanks to Dan Bradley for doing way more than your share of the cooking and dishes these past few years, and for always believing in me. Thanks to the best dog ever, Jasper, for making me laugh every single day – and for never actually eating my homework or my hardware.

And finally, I owe a huge thanks to Jim Ewing for being such a patient test pilot during a crazy and hectic year, and for all the time you spent helping make this project a reality. Also thanks for trusting me on belay!

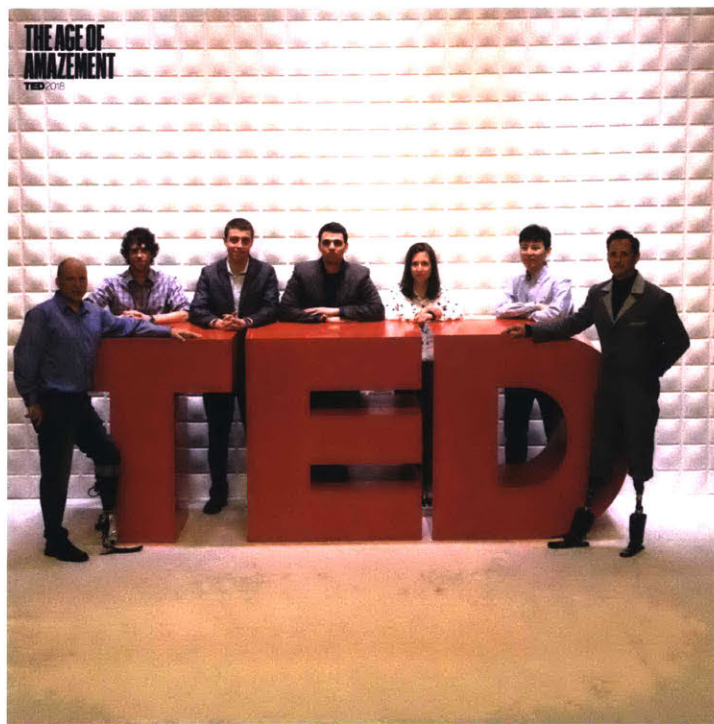


Figure 0-1: **Team Cyborg.** The Biomechatronics crew after Professor Herr's Ted Talk, "How We'll Become Cyborgs and Extend Human Potential" (April 2018).



# Contents

<b>1</b>	<b>Introduction</b>	<b>19</b>
1.1	Motivation . . . . .	19
1.2	Biomechanics . . . . .	20
1.2.1	Ankle-Foot Biomechanics . . . . .	20
1.2.2	Biomechanics of the Knee and Hip . . . . .	20
1.2.3	Biomechanics of Rock Climbing . . . . .	21
1.3	Prior Art . . . . .	21
1.3.1	Climbing Specific Prostheses . . . . .	21
1.3.2	Passive Walking Prostheses . . . . .	22
1.3.3	Powered and Quasi-Passive Walking Prostheses . . . . .	22
1.3.4	Limitations . . . . .	24
1.4	Research Objective . . . . .	25
<b>2</b>	<b>Prosthesis Design</b>	<b>27</b>
2.1	Design Requirements . . . . .	27
2.2	Design Concepts . . . . .	28
2.2.1	Dynamic Actuators . . . . .	29
2.2.2	Clutchable Actuators . . . . .	29
2.2.3	Non-Backdrivable Actuators . . . . .	30
2.2.4	Concept Evaluation . . . . .	30
2.3	System Overview . . . . .	30
2.4	Mechanical Design . . . . .	33
2.4.1	Ankle-Foot Prosthesis . . . . .	33

2.4.2	Linear Actuator Design . . . . .	37
2.5	Control System Design . . . . .	41
2.5.1	Virtual Joint Model . . . . .	43
2.5.2	Position Controller . . . . .	43
2.6	Electronics Design . . . . .	44
2.6.1	Embedded System . . . . .	44
2.6.2	Motor Selection . . . . .	44
2.6.3	Sensors . . . . .	45
2.6.4	Lithium Polymer Battery . . . . .	46
2.6.5	EMG Acquisition and Processing . . . . .	46
2.7	Design Details . . . . .	48
2.7.1	Range of Motion . . . . .	48
2.7.2	Mass and Dimensions . . . . .	51
2.7.3	Torque and Power . . . . .	52
2.7.4	Structural Optimization . . . . .	56
<b>3</b>	<b>Results</b>	<b>59</b>
3.1	Device Validation . . . . .	59
3.1.1	Mass . . . . .	59
3.1.2	Range of Motion . . . . .	61
3.1.3	Control System . . . . .	61
3.1.4	Electronics . . . . .	62
3.2	Clinical Evaluation . . . . .	65
3.2.1	Experimental Design . . . . .	65
3.2.2	Results . . . . .	68
3.3	Discussion . . . . .	71
<b>4</b>	<b>Conclusions</b>	<b>73</b>
4.1	Thesis Contributions . . . . .	73
4.2	Future Work . . . . .	73

**A Engineering Drawings** **75**

**Bibliography** **87**



# List of Figures

0-1 <b>Team Cyborg.</b> The Biomechatronics crew after Professor Herr's Ted Talk, "How We'll Become Cyborgs and Extend Human Potential" (April 2018). . . . .	5
1-1 <b>Biomechanics of ankle foot complex.</b> The talocrural joint (ankle joint) is responsible for the motions of plantar flexion (toe down) and dorsiflexion (toe up). The subtalar joint is responsible for inversion (toe towards body), and eversion (toe away from body). . . . .	20
1-2 <b>Biomechanics of hip and knee.</b> The knee is a 1-DOF joint, flexing (foot towards body), and extending (foot away from body). The hip is a complex joint, moving in flexion (knee towards front of body), extension (knee towards back of body), abduction (leg out away from center of body), and adduction (leg towards center of body). . . . .	21
1-3 <b>Passive rock climbing prostheses.</b> Existing prostheses designed specifically for rock climbing include commercially available rigid foot prostheses (1-3a, 1-3b, and 1-3c), and a prototyped ankle prosthesis with an articulated spring-driven ankle (1-3d). No device exists that allows the user to volitionally re-position the foot during climbing. . . . .	22
1-4 <b>Existing powered and quasi-passive walking prostheses.</b> Current devices aim to emulate level ground walking gait by injecting power into the stride and modulating ankle angle during stance and swing. These devices are tuned for level ground walking and do not allow the user to directly modulate joint angle. . . . . . . . . . .	23

2-1	<b>Initial design concepts for actuator architecture.</b> High level actuator architecture concepts; dynamic actuator, clutchable actuator, and non-backdrivable actuator. . . . .	28
2-2	<b>Robotic ankle-foot prosthesis.</b> Final system showing 2-DOF ankle-foot prosthesis, linear actuators, rock climbing foot, embedded system, carbon fiber prosthetic socket, and EMG processing board [©Andy Ryan]. . . . .	31
2-3	<b>Control paradigm.</b> When the ankle-foot prosthesis is off the climbing wall, the user is able to modulate foot position with free-space position control. When the device is supporting body weight the non-backdrivable transmission locks the ankle position in place. . . . .	32
2-4	<b>System overview.</b> Model of bionic climbing ankle showing subsystems of device: linear actuators, custom rock climbing foot, 2-DOF ankle U-joint, actuator mounting bracket, electronics, and protective cover. . . . .	33
2-5	<b>Ankle-foot prosthesis assembly.</b> Exploded view showing components of ankle-foot prosthesis assembly. The system consists of two linear actuators, a mounting bracket, ankle joint, foot plate, climbing foot, pyramid adapter, prosthetic pylon, embedded system, heat sink, electronics case, and protective cover. . . . .	34
2-6	<b>Ankle-foot prosthesis motion.</b> The four major motions of the ankle-foot prosthesis: (a) dorsiflexion occurs when both actuators extend, (b) plantar flexion occurs when both actuators contract, (c) eversion occurs when the left actuator contracts and the right actuator extends, and (d) inversion when the left actuator extends and the right actuator contracts. . . . .	36
2-7	<b>2-degree-of-freedom U-joint.</b> A custom U-joint replaces the biological function of the ankle and subtalar joint. The foot plate and ankle mount form a U-joint with a bronze block in the center. Dowel pins are pressed through the holes into the block. . . . .	36

2-8	<b>Custom linear actuator design.</b> Non-backdrivable linear actuator design, exploded view shows all components; U-joint attachment, load cell, motor housing, brushed DC motor, motor mount, shaft coupler, bearing housing, angular contact bearings, bearing adapter, ACME lead screw, actuator hosing, anti-backlash nut, wave spring, nut. . . .	37
2-9	<b>Angular contact bearing configuration.</b> Details of angular contact bearing installment: (a) angular contact bearings are pressed onto an adapter on the screw in the back-to-back configuration, (b) the screw is inserted into the bearing housing and screwed into the flexible shaft coupler, and (c) the bearing housing and actuator housing are screwed together, preloading the bearings. (d) shows a section view of the bearing stack. The shaft coupler and bearing adapter preload the inner races, and the bearing housing and actuator housing preload the outer races. . . . .	38
2-10	<b>Actuator U-joint attachment method.</b> (a) Close up of connection between the ACME nut of the linear actuator and the footplate. attachment design. (b) Exploded view showing dowel pins extracted from the U-joint block prior to assembly. . . . .	38
2-11	<b>Backlash reduction system.</b> A secondary anti-backlash nut is preloaded against the primary nut with a wave spring. The wave spring is compressed during assembly, applying force to the nut and anti-backlash nut in opposing directions. This force maintains contact between the nuts and the ACME screw, reducing backlash in the transmission. . . . .	39
2-12	<b>Actuator housing.</b> The actuator housing, bearing housing, and motor housing thread together during assembly. Flanges on the motor mount interface with slots in the motor housing to prevent the motor from rotating in the actuator. . . . .	39

2-13 <b>Motor mount.</b> The brushed DC motor is bolted to the motor mounting plate. The motor mount has flanges that interface with slots in the motor housing. The motor housing and bearing housing are screwed together, applying a compressive force to the motor mount. This prevents the reaction torque of the motor from spinning the motor during actuation. . . . .	40
2-14 <b>Finite-state machine.</b> High level finite-state machine includes two states: State 1 when the ankle-foot prosthesis is supporting body weight and the joint position is locked, and State 2 when the ankle-foot prosthesis is in free space and neural inputs control position of the foot. Measured torque is compared against a torque threshold to trigger state transitions. . . . .	41
2-15 <b>Control system diagram.</b> Schematic of control system running on device. Three stages of processing are taking place; EMG processing, position control, and device output. State information is sent from the motor encoders back to the position controller to control actuator output. . . . .	42
2-16 <b>Virtual joint model.</b> Block diagram of virtual joint model running on control system. Surface electrodes measure muscle activation signals from the residual limb, send the EMG values through a virtual joint model, output desired joint torque which is sent to a dynamic prosthesis model. . . . .	43
2-17 <b>Position controller.</b> The desired joint angles determined by the virtual joint model are sent to a PID controller on the embedded system. A PWM signal is sent to the actuators to reach the target position. Motor encoder values are converted to actual joint angles to compare against the desired angle. . . . .	44
2-18 <b>FlexSEA pocket embedded system.</b> Custom embedded system designed specifically for wearable robotic applications. The board contains motor drivers, analog inputs, power management electronics, and Bluetooth communication capability. . . . .	45

2-19 <b>EMG liner.</b> The custom EMG liner is fabricated with fabric based dry electrodes in the silicone. This liner ensures repeatable placement of the electrodes for subsequent donnings, and provides a reliable muscle actuation signal for the EMG board. . . . .	47
2-20 <b>EMG platform.</b> The portable EMG acquisition and processing platform installed on a custom-built socket. The EMG board reads muscle activation signals from the custom liner, filters and processes the signal, and sends the processed signals to the embedded system. . . . .	48
2-21 <b>Calculating actuator length for given talocrural angle and subtalar angle.</b> Euler rotation matrices are used to calculate the necessary linear travel of the actuators to achieve desired range of motion. . . . .	49
2-22 <b>Actuator length for given talocrural angle and subtalar angle.</b> Actuator length in millimeters is displayed as a color gradient on the plot with talocrural angle on the x-axis and subtalar angle on the y-axis. . . . .	51
2-23 <b>Anthropometry.</b> Average limb segment length as a fraction of total body height was used to determine anthropomorphic dimensions of the ankle-foot prosthesis. . . . .	52
2-24 <b>Transmission ratio.</b> Actuator transmission ratio for given talocrural angle and subtalar angle. As the ankle angle increases, the effective moment arm on the foot decreases, decreasing the transmission ratio. . . . .	55
2-25 <b>Finite element analysis.</b> FEA was performed on all components. A representative result from the FEA performed on the ACME nut is shown here. The gradient of colors corresponds to level of stress in the component for the expected loading conditions. . . . .	57
3-1 <b>Range of motion.</b> Ankle-foot prosthesis range of motion. Each point indicates the coordinates of a position reached, with the subtalar joint angle plotted on the x-axis and the ankle joint angle plotted on the y-axis. . . . .	62

3-2	<b>Actuator step response.</b> Response time of position controller to step input (dashed black). Ankle angle (blue) 13 degrees dorsiflexion to -15 degrees plantar flexion, at a frequency of 1/3 Hz. . . . .	63
3-3	<b>Current, joint angle, and power through 4 cycles.</b> Motor current (amps), joint angle (degrees), and power (watts) averaged for two cycles of 13 degrees dorsiflexion to -15 degrees plantar flexion at a frequency of 1/3 Hz. . . . .	64
3-4	<b>Agonist-antagonist myoneural interface.</b> The subject for this study was a recipient of the agonist-antagonist myoneural interface amputation. This surgical technique preserves the agonist-antagonist relationship between muscles and maintains clear neural signals and proprioceptive feedback, allowing for robust control of robotic prostheses. . . . .	65
3-5	<b>EMG and goniometer sensor placement.</b> Ankle, knee, and hip goniometers placed on a control subject prior to evaluation. EMG muscle sensors are placed on the major muscle groups of the lower extremity. . . . .	66
3-6	<b>Clinical evaluation.</b> Biomechanical data collection while climbing with powered ankle-foot prosthesis and passive rock climbing prosthesis. The subject climbed a 5.10a route in an indoor rock climbing gym while on a top rope belay. . . . .	67
3-7	<b>Joint angles with passive prosthesis and powered prosthesis.</b> Joint angles of the ankle, knee, and hip during rock climbing with the passive prosthesis (blue), and the powered prosthesis (black). The trials are averaged and the standard deviation is shown in shading. . . . .	69
3-8	<b>Joint angles of control subjects.</b> Ankle, knee, and hip angles during rock climbing of Control 1 (blue), Control 2 (black), and Control 3 (yellow). The trials for each subject are averaged and the standard deviation is shown in shading. . . . .	70

# List of Tables

1.1	<b>Prior art.</b> Specifications of existing transtibial prostheses. Mass, powered degrees of freedom, build height, and control scheme. . . . .	24
2.1	<b>Design requirements for bionic climbing prosthesis.</b> Design requirements and specifications for most critical functional requirements. . . . .	28
2.2	<b>Pugh matrix.</b> Rankings of design concepts based on their ability to achieve the design requirements. + indicates the concept fares favorably for that property, - indicates the concept does not achieve that property, and 0 indicates the concept is neutral for that property. The sum of positive and negative attributes is totaled, and the non-backdrivable actuator is determined to be the best design concept. . . . . . . . .	29
2.3	<b>Control system characteristics.</b> State, power consumption, and torque during each of the 2 states in the finite state machine. . . . .	42
2.4	<b>Motor specifications.</b> Characteristics of Maxon DCX 22S brushed DC motor. . . . . . . . .	46
2.5	<b>Parameters for torque and power calculations.</b> The parameters used in the calculations in Section 2.7.3. . . . . . . . .	56
3.1	<b>Final design specifications.</b> Initial requirements and resulting measured values for bionic climbing prosthesis. . . . . . . . .	59
3.2	<b>System mass.</b> Final mass of each component, actuator assembly, and total device mass. The system weight is within the design specification, but can be further reduced by reducing the mass of the climbing foot or by using a smaller lithium polymer battery. . . . . . . . .	60

3.3 <b>Sensor placement during evaluation.</b> EMG sensor placement and goniometer sensor placement during human subject testing. Sensor placement was focused on the left leg as that is the side of amputation for the test subject. . . . .	66
3.4 <b>Subjects for clinical evaluation.</b> Physical characteristics of test subject and control subjects. The control subjects were selected based on their similar height, weight, and climbing ability to the test subject. . . . .	67
3.5 <b>Maximum joint angles.</b> Maximum average joint angle for plantar flexion, dorsiflexion, inversion, eversion, knee flexion, hip flexion, abduction, and adduction while climbing. . . . .	68

# Chapter 1

## Introduction

### 1.1 Motivation

Current lower extremity prosthesis research and development largely focus on the design and control of devices to increase mobility and improve function during activities of daily living such as walking, ascending stairs, and descending stairs. These devices allow persons with lower limb amputation to walk over level ground and variable terrain with gait patterns indistinguishable from those of people with intact biological limbs [1]. However, current robotic prostheses are optimized for level ground walking, and users are unable to efficiently and comfortably perform other recreational and athletic activities. Physical activity has a positive effect on physical and psychological health, but participation in sports and physical activities decreases by an average of 86% following lower limb amputation [2]. For many individuals with lower extremity amputation, their prosthesis technology is a barrier to participation in sports [3]. Despite advances in rehabilitation technology and prosthesis design, 60% of persons with physical impairment do not participate in regular sporting activities [4]. There are numerous benefits of participation in athletics, including: exercise endurance, strength, cardiovascular health, balance, motor skills, improved self image, body awareness, motor development, mood, decreased cardiac risk factors, and improved proficiency in the use of prostheses [4]. Specialized prostheses have been designed for running, cycling, golf, alpine skiing, Nordic skiing, snowboarding, and swimming, but available

technology for adaptive rock climbing is extremely rudimentary.

## 1.2 Biomechanics

### 1.2.1 Ankle-Foot Biomechanics

The biomechanics of the ankle-foot complex are described in Fig. 1-1. The talocrural joint and the subtalar joint are the major joints in the ankle-foot complex. The talocrural joint is responsible primarily for plantar flexion (planting the toe) and dorsiflexion (raising the toe) as shown in Fig. 1-1a. The subtalar joint is responsible for inversion (pointing the foot inward) and eversion (pointing the foot outward), as shown in Fig. 1-1b (adapted from [5]).

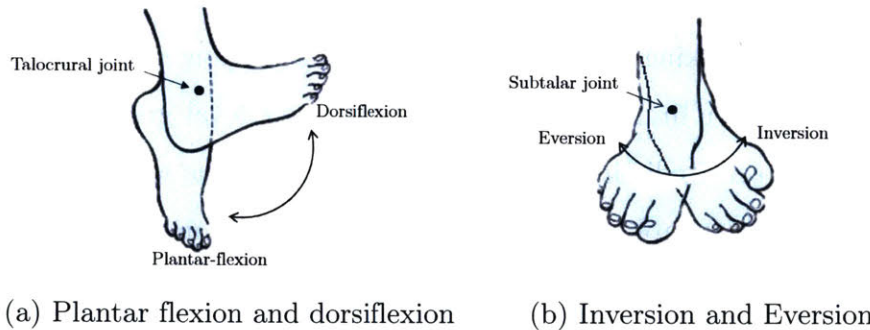
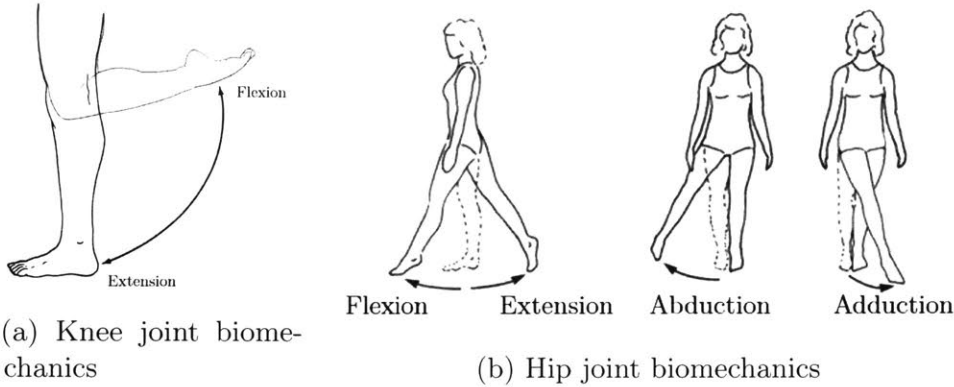


Figure 1-1: **Biomechanics of ankle foot complex.** The talocrural joint (ankle joint) is responsible for the motions of plantar flexion (toe down) and dorsiflexion (toe up). The subtalar joint is responsible for inversion (toe towards body), and eversion (toe away from body).

### 1.2.2 Biomechanics of the Knee and Hip

Standard terminology referring to motions of the hip and knee complexes are outlined in Fig. 1-2. Knee flexion and extension, and hip flexion, extension, abduction, and adduction will be referenced during the biomechanics analysis in Section 3.2.2.



**Figure 1-2: Biomechanics of hip and knee.** The knee is a 1-DOF joint, flexing (foot towards body), and extending (foot away from body). The hip is a complex joint, moving in flexion (knee towards front of body), extension (knee towards back of body), abduction (leg out away from center of body), and adduction (leg towards center of body).

### 1.2.3 Biomechanics of Rock Climbing

Limited research exists on the biomechanics of rock climbing. Research has shown the importance in foot position for climbing ability. Orientation of the ipsilateral foot has been shown to cause statistically significant differences in center of mass and body geometry while climbing [6]. This indicates the importance of controlling position of the ankle-foot complex while climbing.

### 1.3 Prior Art

Prior art includes climbing-specific foot prostheses, passive ankle-foot walking prostheses, and powered ankle-foot walking prostheses.

### 1.3.1 Climbing Specific Prostheses

The commercially available options for prostheses designed specifically for rock climbing are extremely limited. Existing devices include the El Dorado Z-axis foot (Fig. 1-3a), the Evolv adaptive foot (Fig. 1-3b), and the ADK Rock climbing foot (Fig. 1-3c) [7] [8] [9]. These devices are all designed with similar architecture, consisting of a small lightweight foot rigidly fixed at the ankle. These devices are foot prostheses,

passive devices that attach to a standard prosthetic pylon with a rigid, fixed ankle position. Another device designed specifically for rock climbing is the Klippa ankle (Fig. 1-3d) [10]. This device is currently in the prototyping phase and has a passive, 1-degree-of-freedom (DOF) spring-driven articulated ankle.

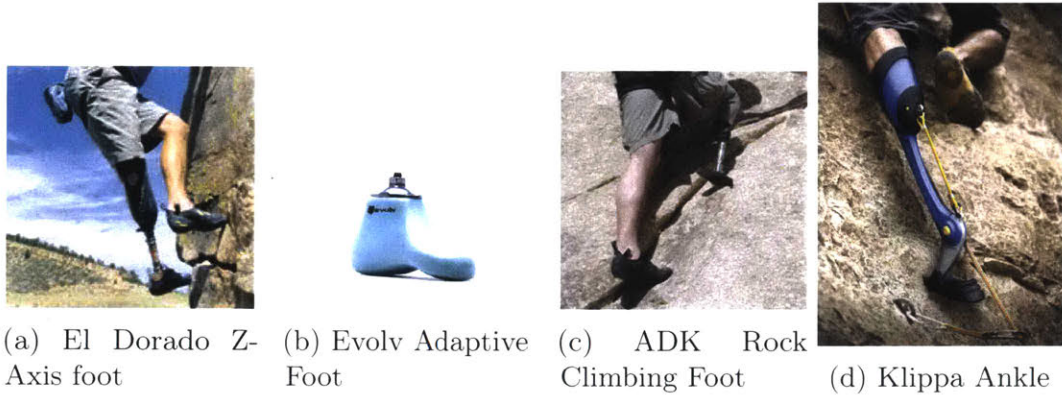


**Figure 1-3: Passive rock climbing prostheses.** Existing prostheses designed specifically for rock climbing include commercially available rigid foot prostheses (1-3a, 1-3b, and 1-3c), and a prototyped ankle prosthesis with an articulated spring-driven ankle (1-3d). No device exists that allows the user to volitionally re-position the foot during climbing.

### 1.3.2 Passive Walking Prostheses

Passive walking prostheses include conventional prostheses and energy-storing-and-returning (ESR) feet. Conventional prosthetic feet include the solid ankle cushioned-heel (SACH) foot, which absorbs ground reaction force upon heel strike through a compressible heel wedge, and the Single-Axis foot, which allows the foot to plantar flex during the early stance phase of walking [11]. These devices lack articulated ankle joint complexes and therefore cannot mimic ankle-foot biomechanics of persons with biological limbs.

### 1.3.3 Powered and Quasi-Passive Walking Prostheses

Quasi-passive prostheses have powered components but do not inject additional power into the gait cycle. These devices provide many of the benefits of powered prostheses

while utilizing lower mass and lower profile power supplies and torque generators. The most popular of these devices is the Proprio-Foot designed by Ossur, which automatically adjusts the swing phase ankle angle based on sensor values read by an onboard microcontroller [12]. This device automatically adapts to the terrain such as increasing the ankle dorsiflexion angle during stair ascent, with a maximum angular range of  $29^\circ$  [13] [12]. Another approach is that used by Koniuk, et al. in their quasi-passive device that detects orientation of the shank and ground contact using a plurality of sensors and utilizes an onboard microcontroller to actively tune the dampening of the ankle during walking, to adjust to various ground surfaces [14]. Another such device uses a cam mechanism to automatically adjust the set point of a plantar flexion and dorsiflexion spring based on slope angle [15]. A similar device utilizes a non-backdrivable lead screw to drive the ankle through a cam, adjusting the ankle angle during the swing phase of walking [16].

Powered prostheses are better able to match biological gait, by providing the user with the ability to change ankle position throughout the gait cycle as well as inject power into the stride. The leader in powered ankle prosthesis technology is the Empower ankle by Ottobock [17]. This device injects power into the gait cycle to allow for powered plantar flexion during walking, allowing for walking gaits closer to that of individuals with intact biological limbs [1].



**Figure 1-4: Existing powered and quasi-passive walking prostheses.** Current devices aim to emulate level ground walking gait by injecting power into the stride and modulating ankle angle during stance and swing. These devices are tuned for level ground walking and do not allow the user to directly modulate joint angle.

### 1.3.4 Limitations

The mass, dynamic torque, power consumption, build height, and control paradigm of the existing devices is listed in Table 1.1. Currently no device exists that restores biological function of the ankle-foot complex while rock climbing. Devices designed specifically for rock climbing are extremely limited in functionality and do not allow the user to re-position the foot while climbing. Powered walking prostheses provide the user with increased functionality; however, the large transmissions and high power requirements cause these devices to be too heavy to be practical for use while climbing. Quasi-passive devices provide some of the benefits of powered devices while generally remaining lighter and smaller. However, no quasi-passive device exists that is optimized for rock climbing. In addition, none of the existing devices incorporate a second degree of freedom to replace subtalar joint function or to allow for volitional EMG control to provide the user with direct control over device motion. We present the design of a 2-DOF, EMG-controlled ankle-foot prosthesis that improves climbing performance in an individual with transtibial amputation beyond what is possible with a traditional passive prosthesis. This device is optimized to enhance performance of persons with transtibial amputation while rock climbing, allowing the user to regain mobility in broader areas of life.

Table 1.1: **Prior art.** Specifications of existing transtibial prostheses. Mass, powered degrees of freedom, build height, and control scheme.

Device	Mass (g)	Powered DOF	Build Height (mm)	Control Paradigm
El Dorado Z-Axis Foot	709	0	114	Passive
Evolv Adaptive Foot	758	0	-	Passive
ADK Rock Climbing Foot	1000	0	-	Passive
Klippa Ankle	-	0	-	Spring loaded
Proprio Foot	1424	1	176	State machine
Empower	2200	1	220	State machine

## 1.4 Research Objective

The aim of this thesis is to augment rock climbing ability in persons with transtibial amputation by providing neural control of a 2-DOF prosthesis. We hypothesize that a climbing specific robotic ankle-foot prosthesis will result in more biological emulation than a passive prosthesis. Specifically, we hypothesize that joint angles of the hip, knee, and ankle of a person with transtibial amputation while rock climbing are more similar to the joint angles of a height-, weight-, and ability-matched control subject with intact limbs, than while climbing with a passive prosthesis. To test the hypothesis, a powered, 2-degree of freedom, neurally controlled prosthesis is built that comprises a pair of non-backdrivable linear actuators providing 16 degrees of dorsiflexion, 18 degrees of plantar flexion, and 20 degrees each of inversion and eversion. This thesis presents the design and evaluation of a lightweight, neurally controlled 2-degree of freedom robotic ankle-prosthesis for rock climbing, a biomechanical study of elite rock climbers with intact biological limbs, and comparison of performance of a person with transtibial amputation with a passive prosthesis and powered prosthesis.



# Chapter 2

## Prosthesis Design

### 2.1 Design Requirements

To investigate the effect of a robotic, electromyography (EMG) controlled, position-controlled ankle-foot complex on rock climbing technique and biomechanics, a robotic ankle-foot prosthesis with two actuated degrees of freedom was designed. The mechanical design was guided by the design requirements, shown in Table 2.1. These requirements were determined based on interviews with rock climbers with transtibial amputation, and in order to improve upon existing devices as outlined in Table 1.1. As this device is intended to be used primarily for rock climbing up a vertical wall, keeping the weight to a minimum while allowing for volitional control of foot position is the primary goal. Rock climbing is a unique sport in which the ability to precisely position the foot on holds is more indicative of an elite climber than dynamic strength. As such, the most critical of these requirements is that the device must allow for user-controlled motion about the subtalar and ankle joint axes. The device must also be weigh less than 1400 grams; must provide  $\pm 20^\circ$  of range of motion about each degree of freedom; and must generate sufficient dynamic torque for free space motion of the foot while supporting a 100-kg user during stance.

Table 2.1: **Design requirements for bionic climbing prosthesis.** Design requirements and specifications for most critical functional requirements.

Parameter	Value
Range of Motion	Inversion/Eversion: +/- 20 degrees Plantar flexion/dorsiflexion: +/- 20 degrees
Max Payload	100 kg
Free-space torque	1 Nm
Velocity	1 Rad/s
Mass	< 1400 g
Build height	< 260 mm
Battery life	> 2 hours

## 2.2 Design Concepts

Several design concepts were explored to determine the best approach for achieving the design requirements outlined in Table 2.1. Among these are dynamic actuators, a clutchable actuator system, and a non-backdrivable system.

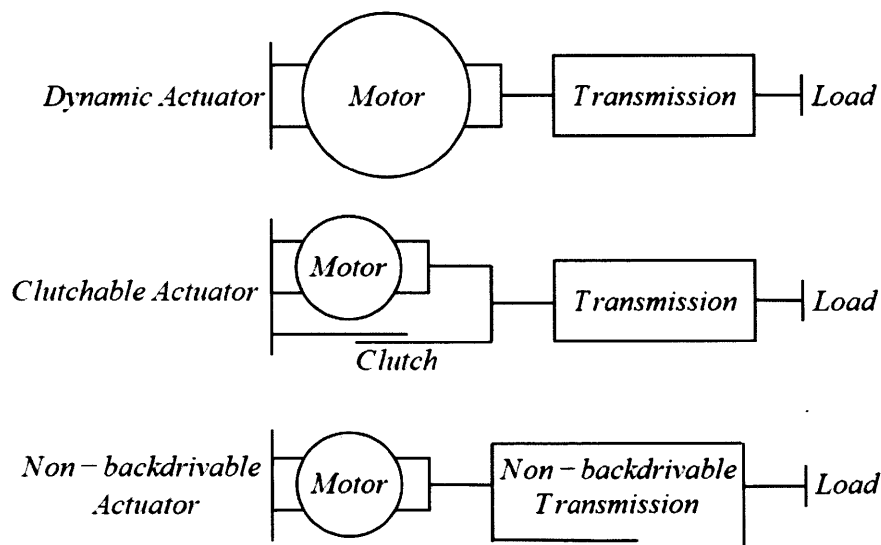


Figure 2-1: **Initial design concepts for actuator architecture.** High level actuator architecture concepts; dynamic actuator, clutchable actuator, and non-backdrivable actuator.

## 2.2.1 Dynamic Actuators

The dynamic actuator concept consists of a transmission in series with the motor that drives the load directly. This actuator requires a higher torque system as even to maintain static positions during stance the system must be able to generate sufficient torque to counteract ankle torque generated by the user's mass. The benefits of this concept are that with a sufficiently sized motor, the system is able to perform dynamic movements. However, this design requires a higher power motor which necessitates heavier components; the increased power consumption leads requires batteries.

## 2.2.2 Clutchable Actuators

In order to reduce the motor size required for the system, a clutchable actuator concept includes a braking mechanism in parallel with the motor. This mechanism allows the motor to be lower power, as the motor does not need to generate sufficient torque to support ankle torque generated by body mass when the clutch is engaged during stance. However, the clutching mechanism adds complexity to the design and control system. In addition, the clutch consumes power.

Table 2.2: **Pugh matrix.** Rankings of design concepts based on their ability to achieve the design requirements. + indicates the concept fares favorably for that property, – indicates the concept does not achieve that property, and 0 indicates the concept is neutral for that property. The sum of positive and negative attributes is totaled, and the non-backdrivable actuator is determined to be the best design concept.

Property	Concept 1: Dynamic	Concept 2: clutchable	Concept 3: Non-backdrivable
Mass	–	0	+
Power consumption	–	–	+
Build height	0	+	+
Torque generation	+	–	–
Complexity/robustness	0	–	+
SUM:	–1	–2	+3
Ranking	2	3	1

### **2.2.3 Non-Backdrivable Actuators**

A second concept that requires less torque generation than the dynamic actuator is a non-backdrivable actuator. This concept utilizes a non-backdrivable transmission, allowing for a low power motor without the need of a energy inefficient, noisy clutch. However, non-backdrivable transmissions are inherently inefficient due to the large amount of friction in the system.

### **2.2.4 Concept Evaluation**

A Pugh chart (Table 2.2) presents the positive and negative attributes of each concept. The non-backdrivable actuator concept compares favorably to the dynamic and clutchable actuators due to its low mass, low power consumption, simplicity, and robustness.

## **2.3 System Overview**

This thesis presents the design of a non-backdrivable 2-degree-of-freedom prosthesis that allows the user to precisely control foot placement while climbing (Fig. 2-2). The device provides the functional benefits of a powered prosthesis while remaining lightweight and low power. The device is designed to provide sufficient torque to move the foot in free space, while supporting full body mass in a static position. This function is achieved with a pair of non-backdrivable linear actuators spanning a 2-DOF gimbal ankle joint. This non-backdrivable design allows for precise free space control of the foot position and a secure ankle-foot position during stance while consuming no additional power (Fig. 2-3). Muscle activation signals are recorded through a custom EMG liner worn on the residual limb, processed on a custom EMG processing board, and sent to an embedded system that computes desired joint output through a virtual joint model and drives the actuators to the desired position. This chapter discusses the design of the non-backdrivable linear actuators, the ankle-foot prosthesis, electronics, and control system.

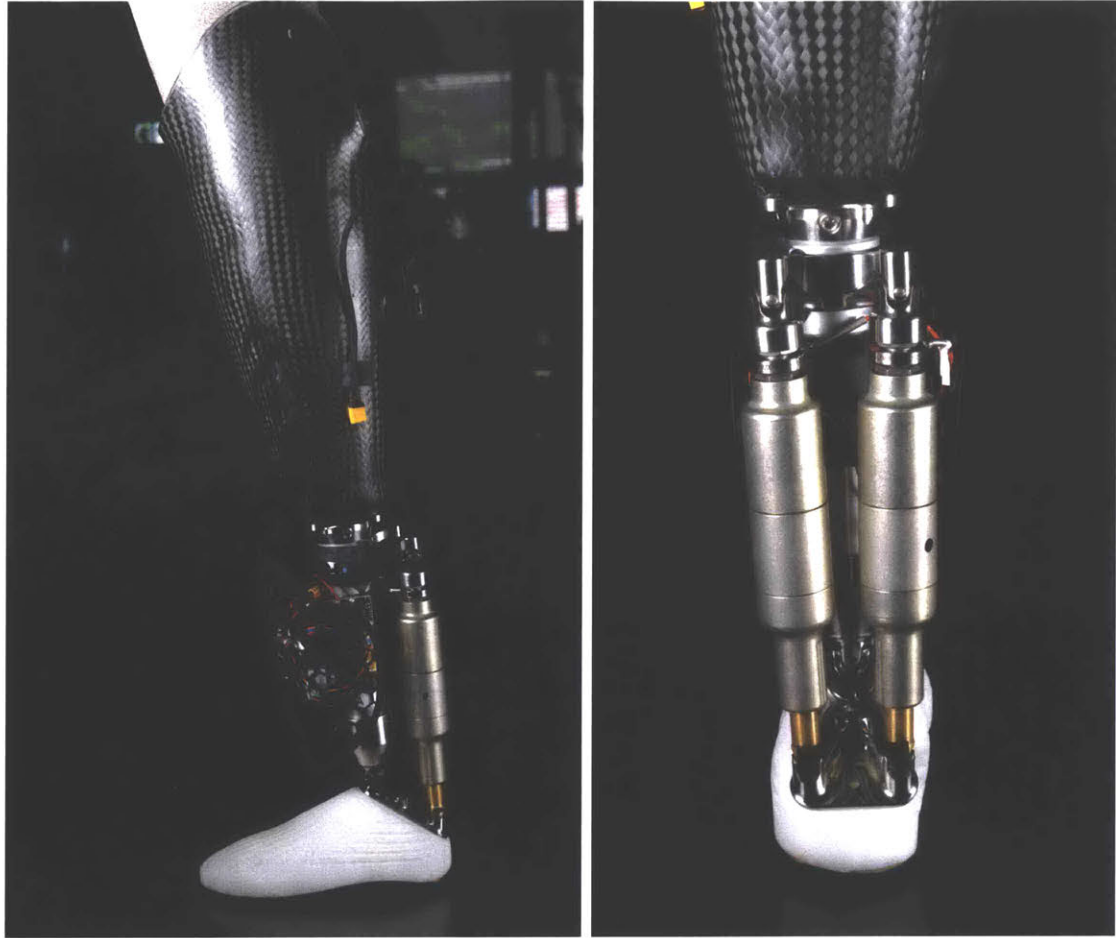


Figure 2-2: **Robotic ankle-foot prosthesis.** Final system showing 2-DOF ankle-foot prosthesis, linear actuators, rock climbing foot, embedded system, carbon fiber prosthetic socket, and EMG processing board [©Andy Ryan].

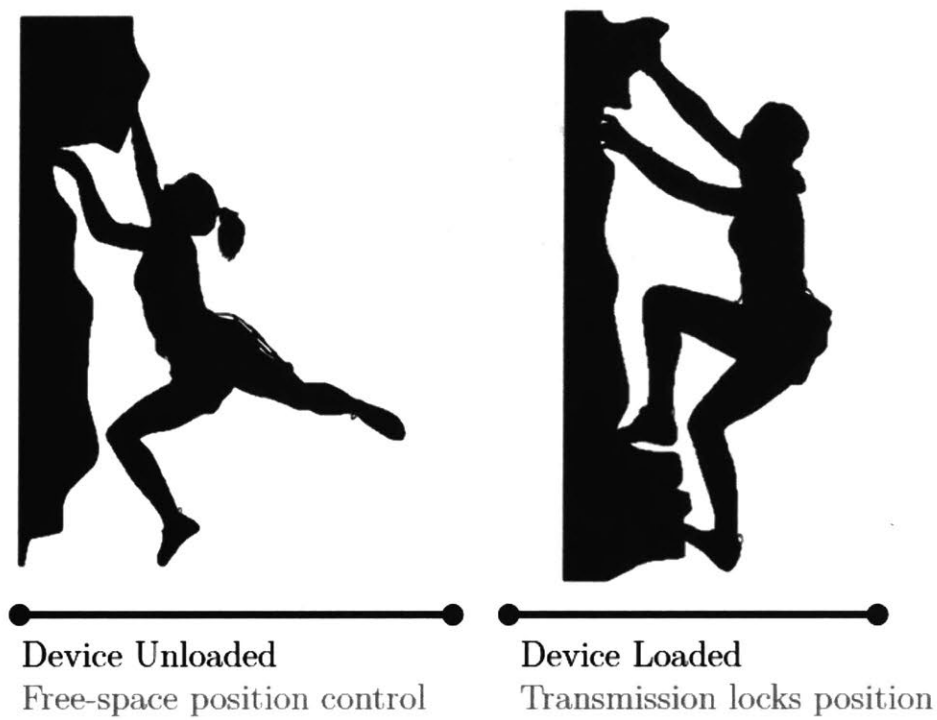


Figure 2-3: **Control paradigm.** When the ankle-foot prosthesis is off the climbing wall, the user is able to modulate foot position with free-space position control. When the device is supporting body weight the non-backdrivable transmission locks the ankle position in place.

## 2.4 Mechanical Design

### 2.4.1 Ankle-Foot Prosthesis

The final ankle-foot prosthesis design is shown in Fig. 2-4: linear actuators, custom climbing foot, 2-DOF U-joint, actuator bracket, electronics, protective cover, prosthesis endoskeletal pylon, and pyramid adapter. Fig. 2-5 shows an exploded view of the ankle-foot prosthesis.

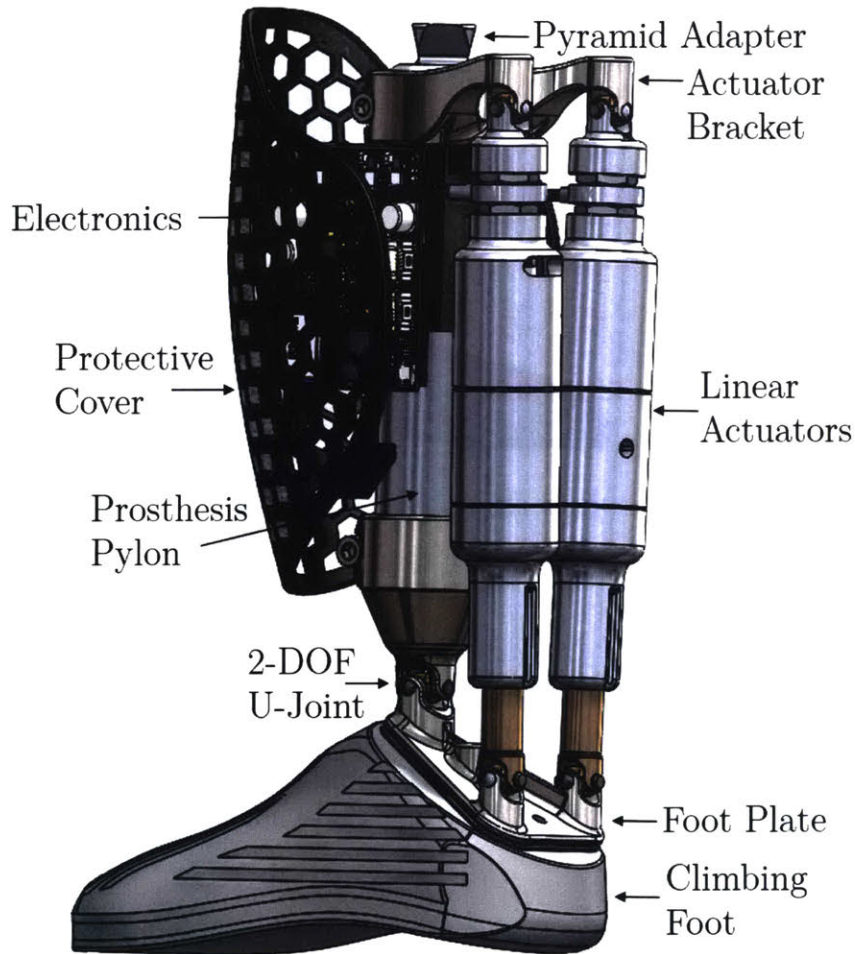


Figure 2-4: **System overview.** Model of bionic climbing ankle showing subsystems of device: linear actuators, custom rock climbing foot, 2-DOF ankle U-joint, actuator mounting bracket, electronics, and protective cover.

The ankle-foot prosthesis utilizes two non-backdrivable custom linear actuators

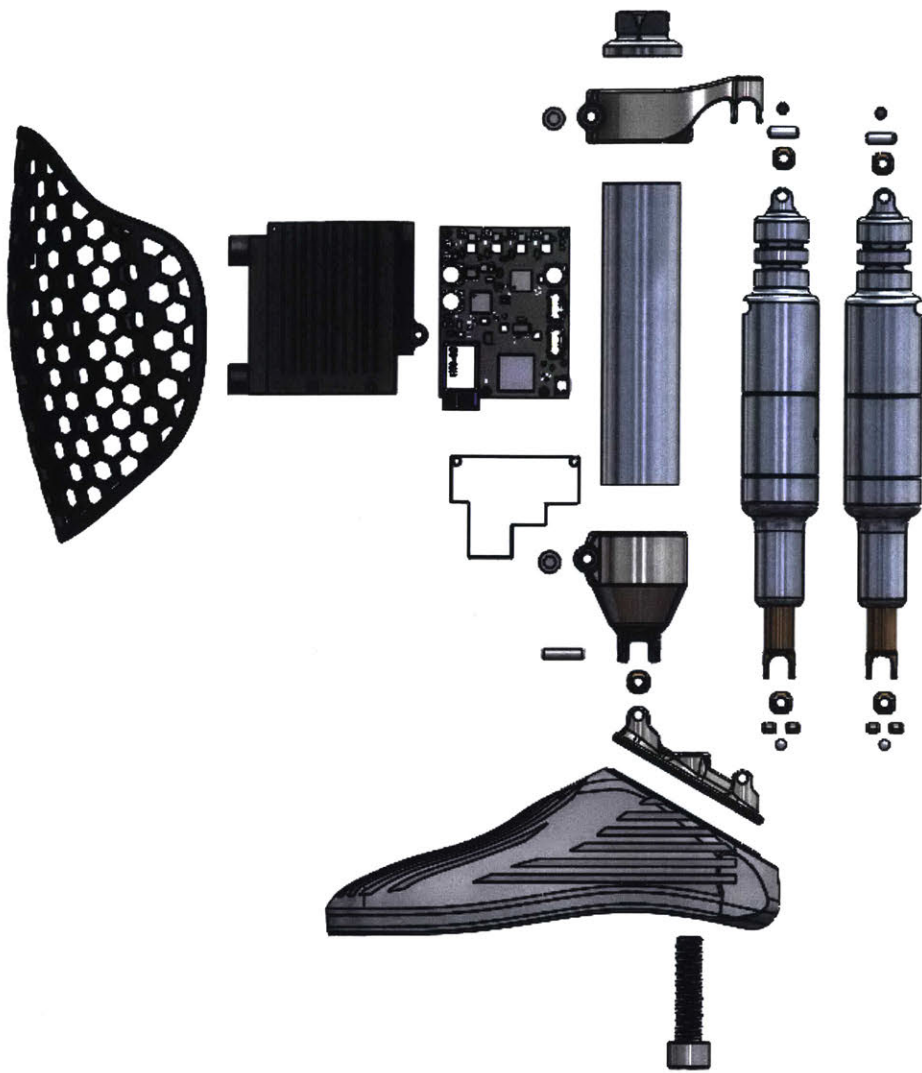


Figure 2-5: **Ankle-foot prosthesis assembly.** Exploded view showing components of ankle-foot prosthesis assembly. The system consists of two linear actuators, a mounting bracket, ankle joint, foot plate, climbing foot, pyramid adapter, prosthetic pylon, embedded system, heat sink, electronics case, and protective cover.

described in detail in Section 2.4.2. A custom titanium mounting bracket, foot plate, and ankle joint attach to a standard prosthesis pylon to form the structure of the ankle-foot prosthesis. A custom rock climbing foot bolts onto the footplate, and an electronics case and protective cover attach to the pylon. The ankle and foot plate components form a 2-axis gimbal U-joint, forming the prosthetic ankle and subtalar joint. This joint allows the foot to plantar flex/dorsiflex, and invert/evert when driven

by the actuators. The actuators are configured in a differential pair; when both actuators actuate in the same direction the ankle-foot prosthesis dorsiflexes (Fig. 2-6a) or plantar flexes and (2-6b). When one actuator contracts and the other extends, the device everts (Fig. 2-6c) or inverts (Fig. 2-6d). The U-joint consists of a custom foot plate and ankle joint attachment, with a bronze block in the center of the joint that dowel pins press into (Fig. 2-7). This forms a secure connection with very little backlash that can be disassembled and reassembled during maintenance or repairs. The climbing foot was designed based on a 3D scan of a rock climbing shoe. The foot is designed to be 40% smaller than the average foot size of a 50th percentile male, to allow the user to precisely place their foot on holds. The foot is selective laser sintered from nylon to allow for the complex geometry in a robust and lightweight package, and climbing shoe rubber attached to the sole. The interface between the climbing foot and the foot plate is at a 30 degree angle, which maximizes the actuator height while reducing overall build height. A nylon electronics case attaches to the pylon to hold the LiPo battery, embedded system, and heat sink. A nylon protective cover attaches to the electronics case to protect the embedded system and analog signal and power wires. The mounting bracket, ankle, and foot plate are machined from 6AL-4V titanium. Engineering drawings of all custom components are included in Appendix A.

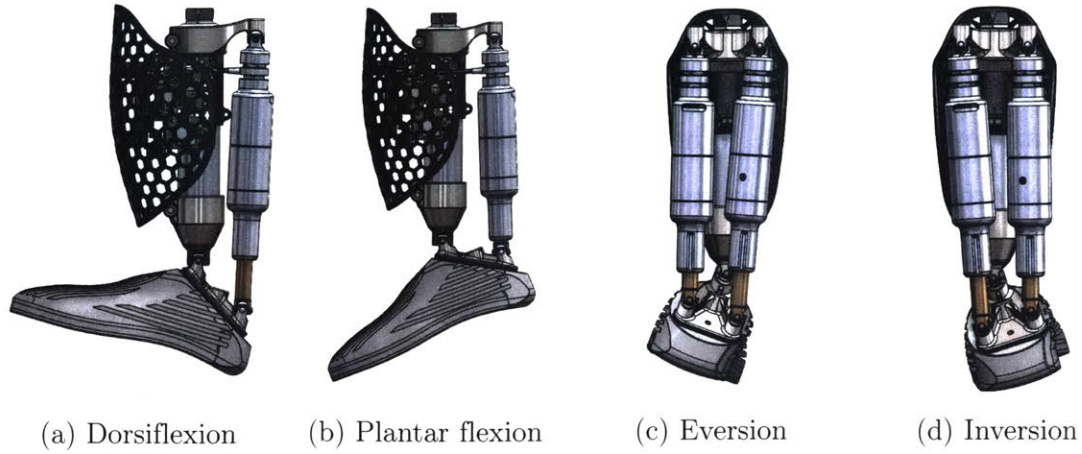
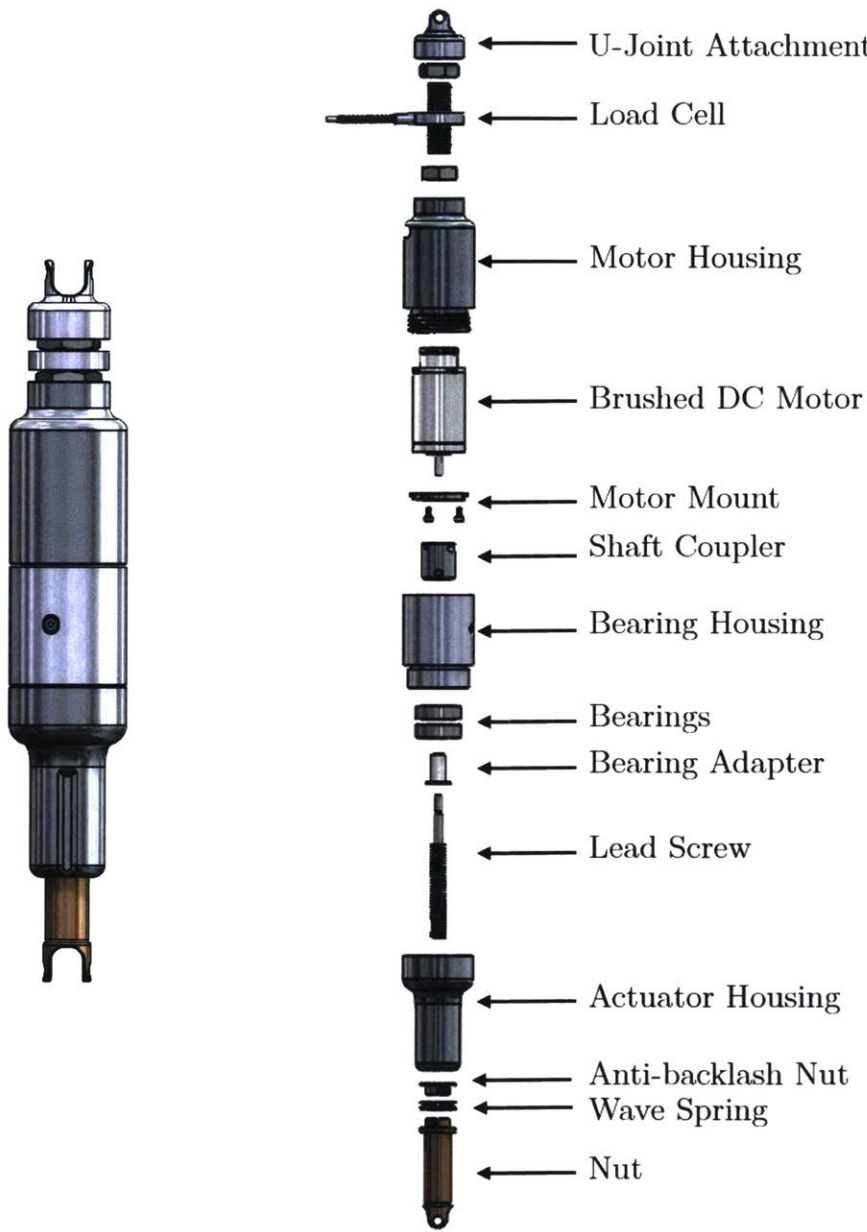


Figure 2-6: **Ankle-foot prosthesis motion.** The four major motions of the ankle-foot prosthesis: (a) dorsiflexion occurs when both actuators extend, (b) plantar flexion occurs when both actuators contract, (c) eversion occurs when the left actuator contracts and the right actuator extends, and (d) inversion when the left actuator extends and the right actuator contracts.



Figure 2-7: **2-degree-of-freedom U-joint.** A custom U-joint replaces the biological function of the ankle and subtalar joint. The foot plate and ankle mount form a U-joint with a bronze block in the center. Dowel pins are pressed through the holes into the block.



**Figure 2-8: Custom linear actuator design.** Non-backdrivable linear actuator design, exploded view shows all components; U-joint attachment, load cell, motor housing, brushed DC motor, motor mount, shaft coupler, bearing housing, angular contact bearings, bearing adapter, ACME lead screw, actuator hosing, anti-backlash nut, wave spring, nut.

#### 2.4.2 Linear Actuator Design

The linear actuator design is shown in Fig. 2-8. A brushed DC motor (Maxon Motor, DCX 22S) drives an ACME thread lead screw (0.0625" lead), which in turn drives

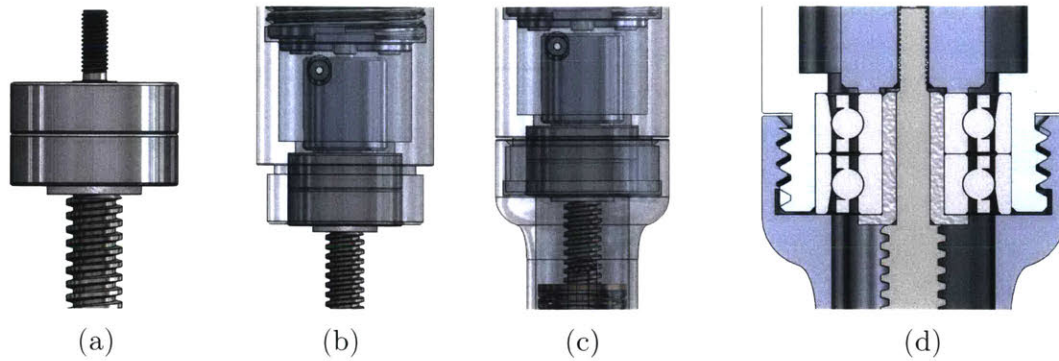


Figure 2-9: **Angular contact bearing configuration.** Details of angular contact bearing installment: (a) angular contact bearings are pressed onto an adapter on the screw in the back-to-back configuration, (b) the screw is inserted into the flexible shaft coupler, and (c) the bearing housing and actuator housing are screwed together, preloading the bearings. (d) shows a section view of the bearing stack. The shaft coupler and bearing adapter preload the inner races, and the bearing housing and actuator housing preload the outer races.

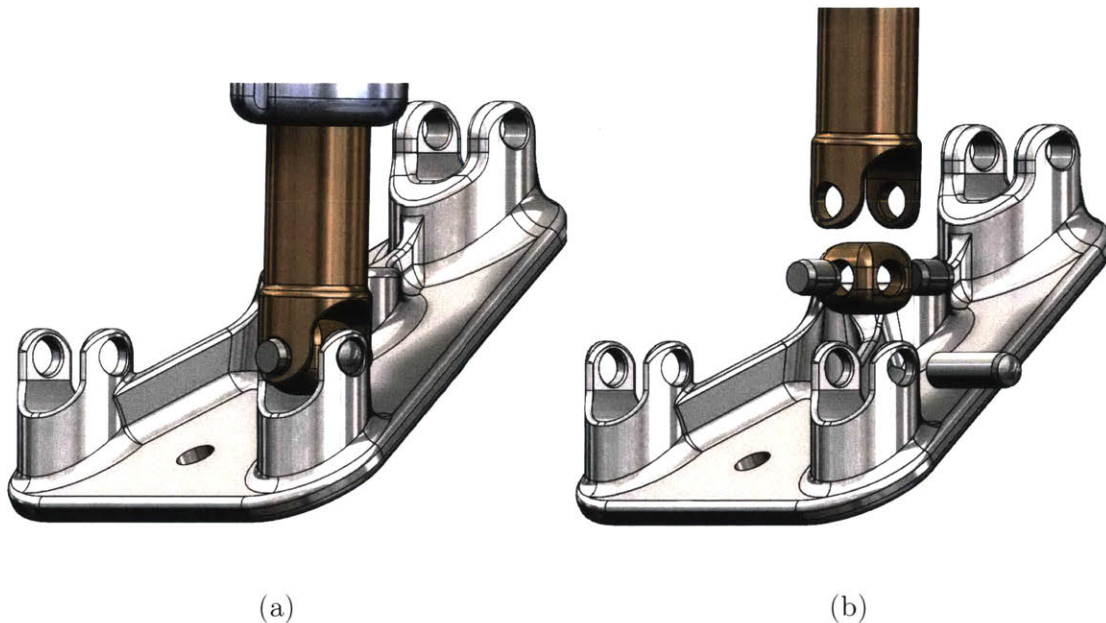


Figure 2-10: **Actuator U-joint attachment method.** (a) Close up of connection between the ACME nut of the linear actuator and the footplate. attachment design. (b) Exploded view showing dowel pins extracted from the U-joint block prior to assembly.

axial translation of the ACME nut. The screw is connected to the motor axle through a custom flexible shaft coupling (Helical). A back-to-back pair of angular contact bearings (GMN, S626) are press fit onto the screw (Fig. 2-9a), which is then inserted



Figure 2-11: **Backlash reduction system.** A secondary anti-backlash nut is preloaded against the primary nut with a wave spring. The wave spring is compressed during assembly, applying force to the nut and anti-backlash nut in opposing directions. This force maintains contact between the nuts and the ACME screw, reducing backlash in the transmission.



Figure 2-12: **Actuator housing.** The actuator housing, bearing housing, and motor housing thread together during assembly. Flanges on the motor mount interface with slots in the motor housing to prevent the motor from rotating in the actuator.

into the bearing housing during assembly (Fig. 2-9b). The inner race of the bearings is preloaded between the bearing adapter and the custom shaft coupling, and the outer race is preloaded between the actuator housing and the bearing housing (Fig. 2-9d). The bearings were selected based on their dimensions and the static radial load rating of 1170 N. The base of the nut is secured to the foot plate through a U-joint, preventing rotation of the nut and constraining the rotation of the motor to produce linear translation of the actuators (Fig. 2-10). The linear actuators interface with the system via U-joint attachment points on the foot plate and mounting bracket. The



Figure 2-13: **Motor mount.** The brushed DC motor is bolted to the motor mounting plate. The motor mount has flanges that interface with slots in the motor housing. The motor housing and bearing housing are screwed together, applying a compressive force to the motor mount. This prevents the reaction torque of the motor from spinning the motor during actuation.

U-joint attachment between the actuator nut and the foot plate prevents the nut from rotating, which forces linear extension and contraction without the need of a linear slide mechanism. A secondary anti-backlash nut is preloaded against the primary nut, compressing a wave spring (Smalley, CMS14-M1), which decreases backlash in the system when it changes direction of travel (Fig. 2-11). A load cell (Futek, LCM200) is mounted in line with each actuator, allowing for accurate sensing of ankle torque. The proximal end of each actuator is attached to a mounting bracket that clamps onto the endoskeletal support pylon. The motor housing, bearing housing, and actuator housing have threads machined into the interface and screw together during actuator assembly (Fig. 2-12). The motor bolts onto the motor mount plate via the bolt pattern in the motor's face. This motor mount has flanges that interface with slots on the motor housing, which is compressed between the motor housing and bearing

housing during assembly, preventing rotation of the motor (Fig. 2-13).

The U-joint attachment, motor housing, motor mount, bearing housing, and actuator housing are precision machined from 7075 aluminum. The lead screw and bearing adapter are machines from alloy steel. The anti-backlash nut and primary nut are machined from 544 bearing bronze to reduce friction in the transmission. The non-backdrivable actuator design allows for high static holding torque without the need of a high-power motor or clutch. Engineering drawings of all custom components are included in Appendix A.

## 2.5 Control System Design

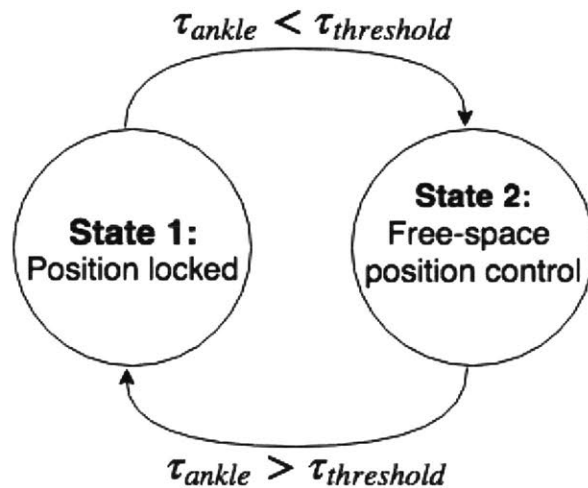


Figure 2-14: **Finite-state machine.** High level finite-state machine includes two states: State 1 when the ankle-foot prosthesis is supporting body weight and the joint position is locked, and State 2 when the ankle-foot prosthesis is in free space and neural inputs control position of the foot. Measured torque is compared against a torque threshold to trigger state transitions.

As demonstrated in Fig. 2-3, the high-level control system operates within two distinct states; when the device is supporting body weight of the user (State 1), and when the device is unloaded in free space (State 2) (Fig. 2-14). When load is detected on the ankle through the load cells, the actuators are turned off, locking the ankle position and withstanding up to 100 Nm of static torque (State 1). When the applied

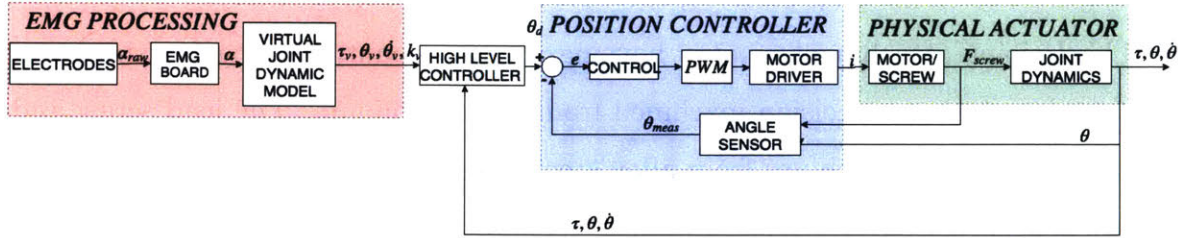


Figure 2-15: **Control system diagram.** Schematic of control system running on device. Three stages of processing are taking place; EMG processing, position control, and device output. State information is sent from the motor encoders back to the position controller to control actuator output.

torque on the ankle is less than the threshold of the system, the actuators provide 1 Nm of dynamic torque in order to re-position the foot according to neural inputs detected from the EMG system (State 2). Table 2.3 outlines the power consumption and torque production in each state.

Table 2.3: **Control system characteristics.** State, power consumption, and torque during each of the 2 states in the finite state machine.

State	Functionality	Power Consumption	Torque
1	Ankle position locked	0 W	100 Nm (static)
2	EMG driven position control	12 W	1 Nm (dynamic)

The device's control system reads biological signals from the residual limb; filters and processes these data; and sends the data to the onboard embedded controller, calculating the target position and velocity and sending commands to the motor. The control system has three stages: EMG processing, position control, and actuator output (Fig. 2-15). During the EMG processing stage, surface electrodes embedded in a silicone liner (Ottobock) detect muscle activation signals from the residual limb. These signals are sent to a custom portable EMG processing board. The board filters and processes the signal and outputs the percent maximum voluntary contraction (MVC) for each muscle. These activation values are inputs for a virtual joint dynamic model. The virtual joint dynamic model calculates intended torque output for the virtual joint and uses that to calculate position and velocity of the robotic ankle. This position target is then fed into the position controller as a pulse width modulation

(PWM) command.

### 2.5.1 Virtual Joint Model

A virtual joint model (Fig. 2-16) interprets the EMG signal and converts it to desired prosthesis behavior [18]. This model uses muscle activation levels to determine intended agonist and antagonist muscle stiffness and acceleration, and uses this to calculate intended torque about the virtual joint. This torque value is applied to a dynamic model of the ankle-foot prosthesis, outputting a target joint angle for each degree of freedom. The target angles are sent to the position controller in the next stage of the control system.

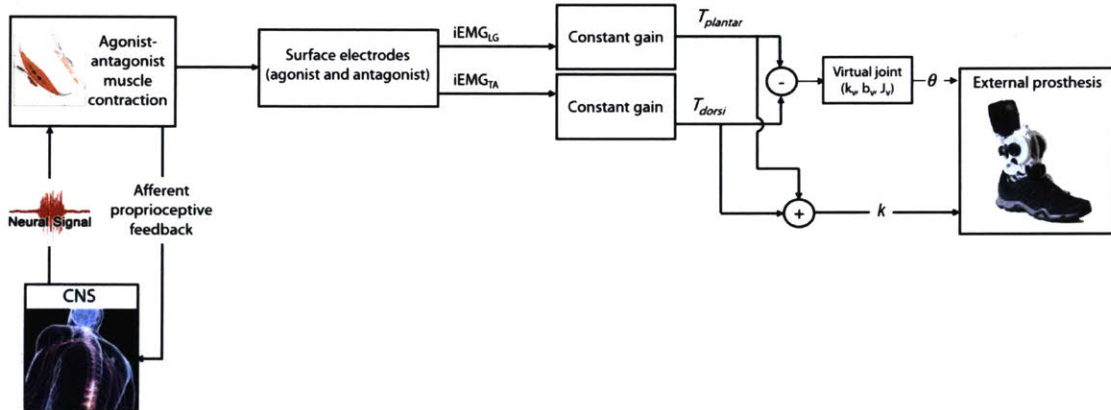


Figure 2-16: **Virtual joint model.** Block diagram of virtual joint model running on control system. Surface electrodes measure muscle activation signals from the residual limb, send the EMG values through a virtual joint model, output desired joint torque which is sent to a dynamic prosthesis model.

### 2.5.2 Position Controller

The position controller receives desired joint angle commands from the virtual joint model, feeds these commands to a PID controller on the embedded system, and sends a PWM signal to each actuator. Sensor feedback is sent from the motor encoders in each actuator, as well as the load cells.

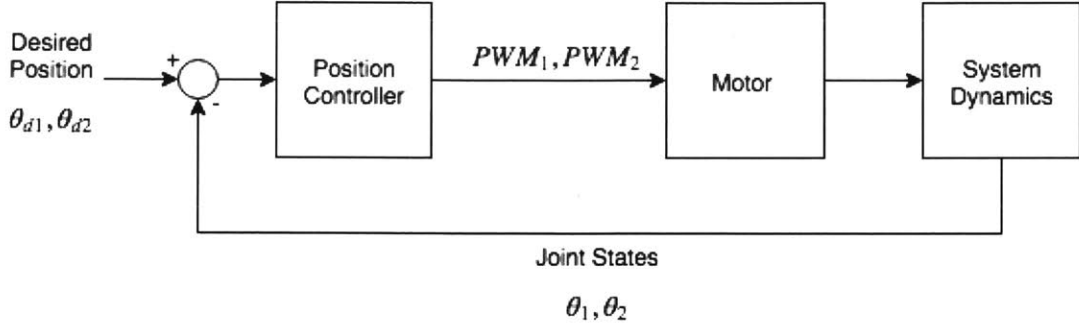


Figure 2-17: **Position controller.** The desired joint angles determined by the virtual joint model are sent to a PID controller on the embedded system. A PWM signal is sent to the actuators to reach the target position. Motor encoder values are converted to actual joint angles to compare against the desired angle.

## 2.6 Electronics Design

### 2.6.1 Embedded System

The prosthesis is controlled by a custom embedded system designed specifically for wearable robotic applications [19]. The FlexSEA Pocket is an embedded system with integrated motor controllers, power management, and a microcontroller (STM 32). The motor controller is programmed using the C programming language. The board is enabled with Bluetooth for real-time monitoring of sensor values and the control loop.

### 2.6.2 Motor Selection

A brushed DC motor (Maxon Motor, DCX 22S) was selected for the actuator design based on the torque and velocity requirements described in Section 2.7.3. The selected motor has graphite brushes, ball bearings, and an integrated optical encoder. The motor was selected based on torque-speed characteristics, size, and price. The specifications of this motor are outlined in Table 2.4.

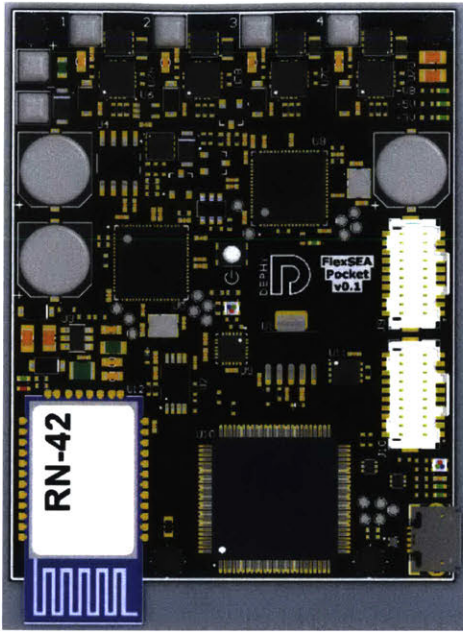


Figure 2-18: **FlexSEA pocket embedded system**. Custom embedded system designed specifically for wearable robotic applications. The board contains motor drivers, analog inputs, power management electronics, and Bluetooth communication capability.

### 2.6.3 Sensors

#### Load Cell

A load cell (Futek, LCM 200) is integrated axially in each actuator, in order to provide accurate torque sensing about the ankle-foot joint. This load cell has a nominal voltage output of 2 mV/V, with non-linearity of +/- 0.5% of the rated output.

#### Motor Encoder

The motor encoder (Maxon Motor, ENX16 EASY 512IMP) is a quadrature incremental optical encoder with 512 counts per turn. The encoder is used to send motor position state to the embedded system. The encoder operates from a supply voltage of 5 V and has a standstill current draw of 23 mA.

Table 2.4: **Motor specifications.** Characteristics of Maxon DCX 22S brushed DC motor.

Specification	Value
Nominal Voltage	12 V
No load speed	12400 rpm
No load current	71.7 mA
Nominal speed	10700 rpm
Nominal torque	14.6 mNm
Nominal current	1.65 A
Stall torque	108 mNm
Stall current	11.8 A
Torque constant	9.18 mNm/A
Speed constant	1040 rpm/V

## 2.6.4 Lithium Polymer Battery

The actuators, EMG system, and embedded system are powered by a single 3 cell lithium polymer battery with a capacity of 800 mAh.

## 2.6.5 EMG Acquisition and Processing

A portable EMG acquisition and processing platform has been developed for active lower-extremity prosthetic system research. The developed platform consists of a specialized prosthetic liner and an embedded electronic system. The specialized prosthetic liner (Ottobock, Inc.) contains 8 bipolar channels of dry fabric EMG electrodes, and the electrodes are physically accessible through an external electrical connector. Fig. 2-19a and Fig. 2-19b show the custom EMG liner.

The embedded EMG electronic system acquires raw EMG signals from the residual limb through the electrical connector on the liner. The embedded system pre-amplifies and digitizes the raw signals, processes the signals with a bandwidth filter of 1kHz on a microprocessor (STM32F405RG-T6), and feeds the signal to the high-level controller on the prosthesis. In order to estimate muscle activation as the percent maximal contraction, the raw EMG signals are filtered with a band-pass filter of 80-420 Hz and averaged with a 100-ms windows. The embedded EMG system feeds the processed EMG data to the device via a I2C communication protocol with a bandwidth of 1



(a) Inner view of the EMG liner with fabric EMG electrodes. (b) Custom EMG liner worn by a subject.

Figure 2-19: **EMG liner.** The custom EMG liner is fabricated with fabric based dry electrodes in the silicone. This liner ensures repeatable placement of the electrodes for subsequent donnings, and provides a reliable muscle actuation signal for the EMG board.

kHz. Fig. 2-20 shows the portable EMG acquisition and processing platform installed on a custom-built socket.

With the portable EMG acquisition and processing platform, muscle signals from the residual limb are accessible in a robust, real-time, fully-portable manner even while the socket is moving and bearing the user's mass.

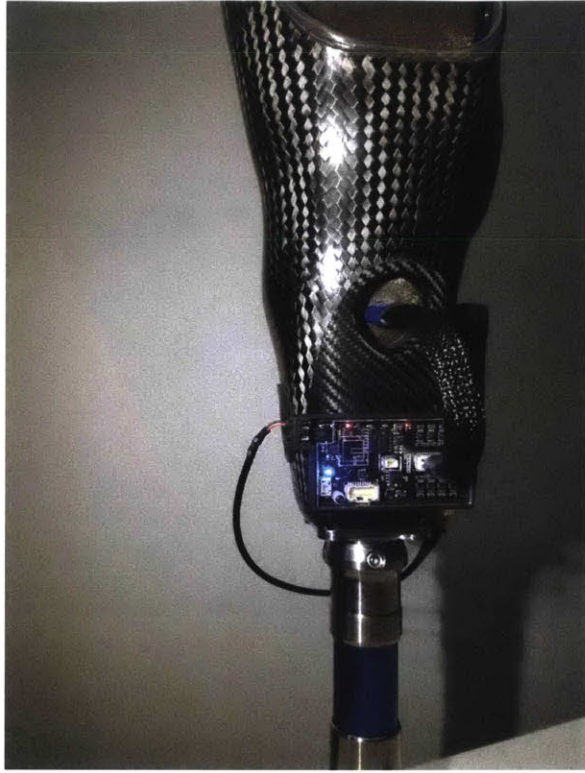


Figure 2-20: **EMG platform.** The portable EMG acquisition and processing platform installed on a custom-built socket. The EMG board reads muscle activation signals from the custom liner, filters and processes the signal, and sends the processed signals to the embedded system.

## 2.7 Design Details

This section describes the detailed design decisions and calculations that led to the final design presented in Sections 2.4, 2.5, and 2.6.

### 2.7.1 Range of Motion

The range of motion of the prosthetic device is determined by the length of travel of the linear actuators and the geometry of the system. The design requirements aim to minimize build height and footprint size while maximizing range of motion. Using the coordinate systems and vectors outlined in Fig. 2-21, we can calculate the length change of the actuators using Euler rotation matrices [20]. As shown in Fig. 2-21,  $l_i$  is the length of the actuator,  $b_i$  is the vector defining the location of the actuator anchor point on the upper attachment bracket,  $T$  is the translation vector that represents the

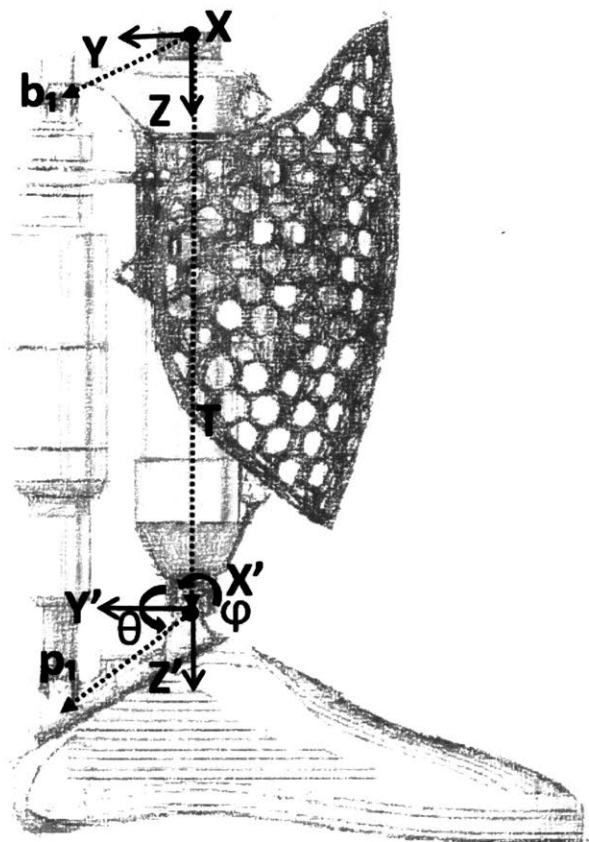


Figure 2-21: **Calculating actuator length for given talocrural angle and subtalar angle.** Euler rotation matrices are used to calculate the necessary linear travel of the actuators to achieve desired range of motion.

position of the foot coordinate system ( $X', Y', Z'$ ) in relation to the base coordinate system ( $X, Y, Z$ ), and  $p_i$  is the initial location of the distal mounting location of the actuator in the foot coordinate system.  $\varphi$  is the angle of motion about the ankle joint, and  $\theta$  is the angle of motion about the subtalar joint. The mounting locations of the actuators are determined by the requirement that the envelope of the device fits inside the area of the lower leg of a 50th percentile male [21].

For our required range of motion of  $\pm 20$  degrees of plantar flexion/dorsiflexion and  $\pm 20$  degrees inversion/eversion, the corresponding actuator length  $l_i$  is calculated. Fig. 2-22 shows the actuator length for a single actuator while the system moves through the range of desired angles, -20 to 20 degrees about the talocrural joint, and -20 to 20 degrees about the subtalar. Fig. 2-22 demonstrates that as the talocrural angle increases, the actuator length required to reach a given subtalar angle increases. Therefore, to keep the build height to within our specifications, we've limited the range of motion to the work space shown in Fig. 2-22, with  $\pm 20$  degrees of inversion and eversion possible at a 0 degree talocrural angle, and  $\pm 10$  degrees at maximum plantar flexion and dorsiflexion. This range compares favorably to the range of motion achieved by the biological ankle-foot complex. On average a biological talocrural joint achieves 10 to 20 degrees of dorsiflexion and 40-55 degrees of plantar flexion, and the subtalar joint allows for 23 degrees of inversion and 12 degrees of eversion [22].

$$R_z(\psi) = \begin{pmatrix} \cos(\psi) & -\sin(\psi) & 0 \\ \sin(\psi) & \cos(\psi) & 0 \\ 0 & 0 & 1 \end{pmatrix}$$

$$R_y(\theta) = \begin{pmatrix} \cos(\theta) & 0 & \sin(\theta) \\ 0 & 1 & 0 \\ -\sin(\theta) & 0 & \cos(\theta) \end{pmatrix}$$

$$R_x(\varphi) = \begin{pmatrix} 1 & 0 & 0 \\ 0 & \cos(\varphi) & -\sin(\varphi) \\ 0 & \sin(\varphi) & \cos(\varphi) \end{pmatrix}$$

$$R = R_x(\varphi) * R_y(\theta) * R_z(\psi)$$

$$l_i = T + R * p_i - b_i$$

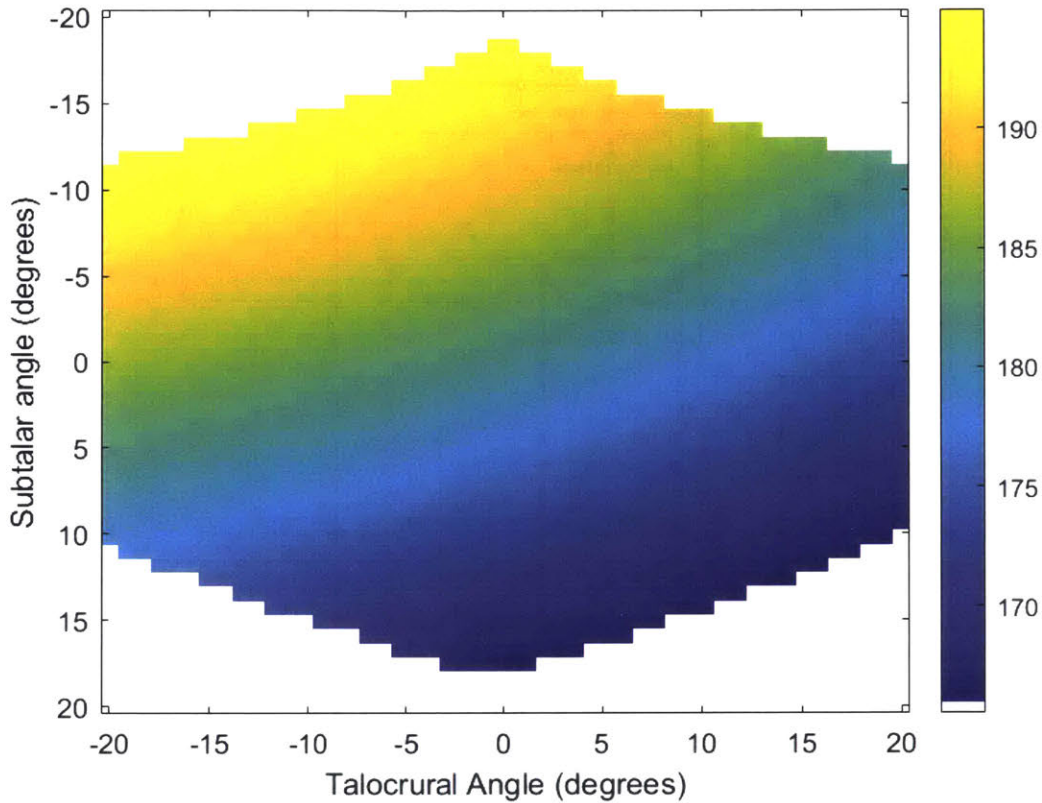


Figure 2-22: **Actuator length for given talocrural angle and subtalar angle.** Actuator length in millimeters is displayed as a color gradient on the plot with talocrural angle on the x-axis and subtalar angle on the y-axis.

### 2.7.2 Mass and Dimensions

The design aims to minimize device mass while achieving the range of motion and torque requirements outlined above. In addition to mass, the dimensions of the system are critical. The build height of the system must be less than the clearance height of the amputation level for any intended user, and the volume of the system should be within the envelope of a typical lower leg and foot segment of a person. Fig. 2-23

shows the average limb lengths as a fraction of total height; lower leg: 0.285, ankle height: 0.039, foot length: 0.152, foot breadth: 0.055 [21]. The segment masses as a portion of total body mass are; foot: 0.0145, leg: 0.0465 [21].

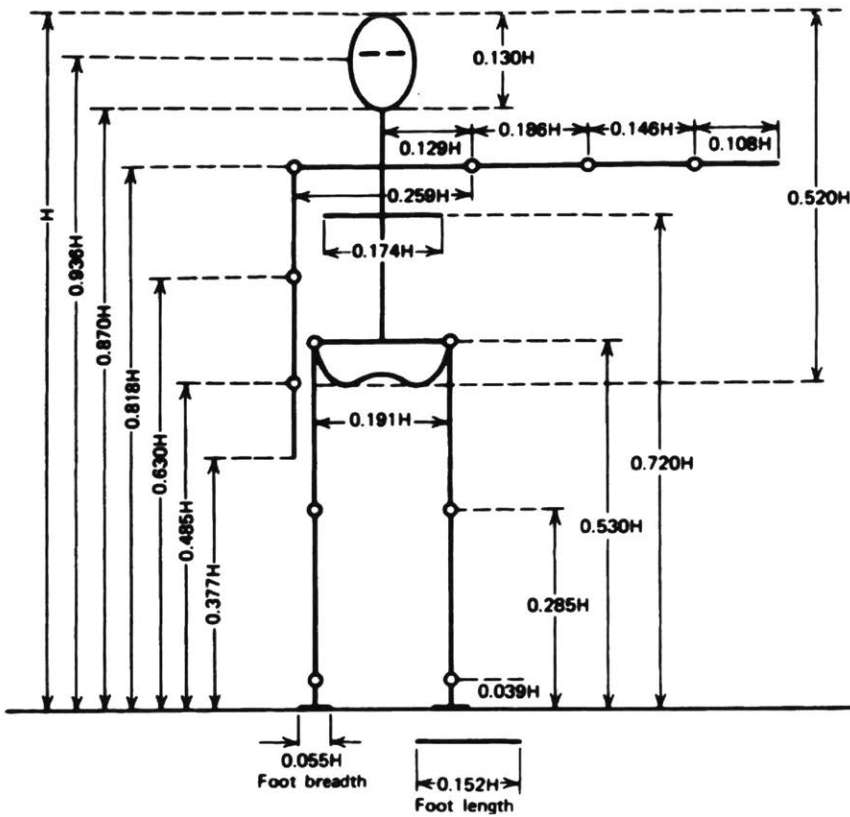


Figure 2-23: **Anthropometry.** Average limb segment length as a fraction of total body height was used to determine anthropomorphic dimensions of the ankle-foot prosthesis.

### 2.7.3 Torque and Power

Another design requirement critical for device performance is that the system must be able to provide sufficient torque to move the foot in free space at the specified angular velocity. The desired angular velocity is 1.0 rad/sec, in order to provide the user with realistic response time of the device. The actuator force and motor torque required for free space motion is calculated as follows:

The total reflected mass moved by each actuator is:

$$m_{total} = m_{nut} + \frac{1}{2} \frac{r_{foot}}{r_{act}} (m_{foot} + m_{fplate}) = 0.411 \text{kg} \quad (2.1)$$

Where  $m_{nut}$ ,  $m_{foot}$ , and  $m_{fplate}$  are the masses of the nut, foot, and footplate respectively.  $\frac{r_{foot}}{r_{act}}$  is the ratio of the radius from the axis of rotation to the center of mass of the foot to the radius from the axis of rotation to the attachment point of the actuator. In reality these distances vary throughout the range of motion of the ankle, but for this calculation it is calculated as fixed. The footplate and foot are each supported by both actuators, so only half of their mass is seen by each actuator.

The axial force on the actuator while moving the foot in free space is calculated in Eqn. 2.2. The total actuator force consists of the force required to accelerate the load, the force required to raise the load against gravity, and the force required to overcome the friction of the transmission.

$$F_{actuator} = F_{accel} + F_{grav} + F_{friction} \quad (2.2)$$

$$F_{actuator} = \frac{m_{total} \alpha_{lin}}{g} + m_{total} g \sin\beta + m_{total} \mu \cos\beta = 2.02 \text{ N}$$

Where  $\alpha_{lin}$  is the linear acceleration of the actuator translation,  $g$  is acceleration due to gravity,  $\beta$  is the thread angle of the ACME screw, and  $\mu$  is the coefficient of friction between the bronze nut and the steel screw.

The necessary torque production by the motor to achieve the desired force output during free space control is calculated as follows:

$$\tau_{motor} = F_{total} \frac{\ell}{2\pi\eta} + J_{screw} \alpha_{screw} = 5.65 \text{ mNm} \quad (2.3)$$

Where  $\ell$  is the lead of the ACME screw,  $\eta$  is the efficiency of the transmission,  $J_{screw}$  is the inertia of the screw, and  $\alpha_{screw}$  is the angular acceleration of the screw.

$$\tau_{ankle} = \begin{cases} 2 F_{actuator} r_{act} = 167.7 \text{ mNm}, & \text{dynamic torque} \\ m_{bw} g r_{foot} = 78.5 \text{ Nm}, & \text{static torque} \end{cases} \quad (2.4)$$

Eq. 2.4 calculates the torque about the ankle joint of the prosthesis during free space motion (dynamic) and during stance (static).  $m_{bw}$  is the mass of the user,  $g$  is acceleration due to gravity, and  $r$  is the radius from the force vector to the joint axis.

The maximum compressive load that the actuators can support is calculated in Eqn. 2.5.  $d_{root}$  refers to the root diameter of the lead screw and  $L$ . The actuator support arrangement is modeled as fixed-free. Each actuator can support a maximum of 9350 N. The maximum compressive load expected on the actuators is 980 N, so there is a safety factor of 19 before shaft buckling is a concern.

$$\text{Critical Load} = 0.25(6.24 * 10^7) \frac{d_{root}^4}{L^2} = 9350 \text{ N} \quad (2.5)$$

The critical speed before shaft whip becomes a concern is calculated in Eqn. 2.6. Shaft whip is a concern when the rotational velocity of the screw is equal to the bending natural frequency of the shaft. The calculated critical speed of 209220 rpm is much higher than the no load speed of the selected motor, 12400 rpm. This indicates that shaft whip is not a concern for this actuator design.

$$\text{Critical Speed} = 0.36(4.76 * 10^6) \frac{d_{root}}{L^2} = 209220 \text{ rpm} \quad (2.6)$$

The effective gear ratio of the system changes throughout the range of motion of the joint, due to the geometry of the system and changing moment arm of ankle. The transmission ratio throughout range of motion is shown in Fig. 2-24. Biologically, the moment arm of the muscles acting on the ankle and subtalar joint vary throughout ankle range of motion as well [23]. This results in variable torque generation for a given muscle force. The transmission ratio,  $N$ , can be calculated as:

$$N = \frac{\omega_{motor}}{\omega_{ankle}} = \frac{2\pi r_{act}(\sin \theta_i - \sin \theta_{i-1})}{\ell \Delta(t)} \quad (2.7)$$

Where  $\omega_{motor}$  is the angular velocity of the motor,  $\omega_{ankle}$  is the angular velocity of the ankle,  $r_{act}$  is the distance between the distal end of the actuator and the axis of rotation,  $\theta$  is the angle between  $r_{act}$  and the vertical axis, and  $\ell$  is the lead of the screw.

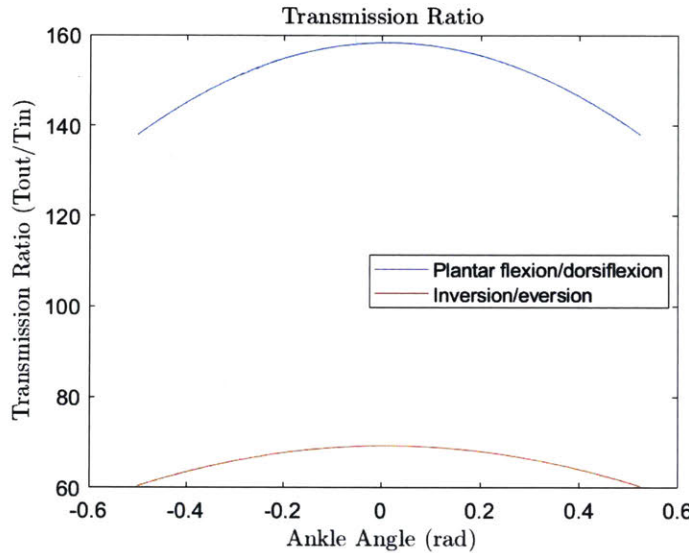


Figure 2-24: **Transmission ratio.** Actuator transmission ratio for given talocrural angle and subtalar angle. As the ankle angle increases, the effective moment arm on the foot decreases, decreasing the transmission ratio.

The mechanical power output of the system is calculated in Eq. 2.8.

$$P = \begin{cases} \omega_{screw} \tau_{motor} = 0.9 W, & \text{dynamic} \\ 0 W, & \text{static} \end{cases} \quad (2.8)$$

Where  $\omega_{screw}$  is the angular velocity of the screw. As the non-backdrivable actuator design does not require any force to maintain constant joint angle, during static loading  $\omega_{screw}$  and  $\tau_{motor}$  are equal to 0. The expected electrical power consumption is approximately 9 watts during free space motion, due to the efficiency rate of the

system. The parameters used to calculate Eq. 2.1 through 2.8 are shown in Table 2.5.

**Table 2.5: Parameters for torque and power calculations.** The parameters used in the calculations in Section 2.7.3.

Parameter	Value	Definition
$m_{bw}$	100 kg	Body mass
$m_{foot}$	0.35 kg	Foot mass
$m_{footplate}$	0.032 kg	Footplate mass
$m_{nut}$	0.029 kg	Nut mass
$m_{screw}$	0.009 kg	Screw mass
$g$	$9.81 \frac{m}{s^2}$	Gravitational acceleration
$r_{foot}$	0.08 m	Radius of foot
$r_{act}$	0.04 m	Radius of actuator
$\alpha_{lin}$	$2 \frac{m}{s^2}$	Linear acceleration
$\beta$	$29^\circ$	Thread angle
$\mu$	0.16	Coefficient of friction (bronze on steel)
$\ell$	$\frac{1}{16}$ inch	Lead of screw
$\eta$	0.10	Efficiency
$J_{screw}$	$4.54 * 10^{-8} kgm^2$	Inertia of screw
$\alpha_{screw}$	$791.6 \frac{rad}{s^2}$	Acceleration of screw
$J_{foot}$	$0.0064 kgm^2$	Inertia of foot
$\alpha_{ankle}$	$5.6 \frac{rad}{s^2}$	Acceleration of foot
$d_{root}$	0.17 inch	Root diameter lead screw
$L$	1.18 inch	Length lead screw
$\theta$	$-\frac{\pi}{9} : \frac{\pi}{9} rad$	Range of ankle angles
$\omega_{ankle}$	$1.0 \frac{rad}{sec}$	Angular velocity of ankle
$\omega_{screw}$	$158 \frac{rad}{sec}$	Angular velocity of ankle

#### 2.7.4 Structural Optimization

The actuator design minimizes device weight while providing sufficient structural integrity to support the payload of the user. The load bearing elements of the actuator are the nut, the bearing housing, the motor housing, and the upper and lower U-joint attachments. The loading conditions of the components were determined using free body diagrams, and finite element analysis was performed to evaluate stress and deflection of critical components. Fig. 2-25 shows a representative result from the finite element analysis (FEA).

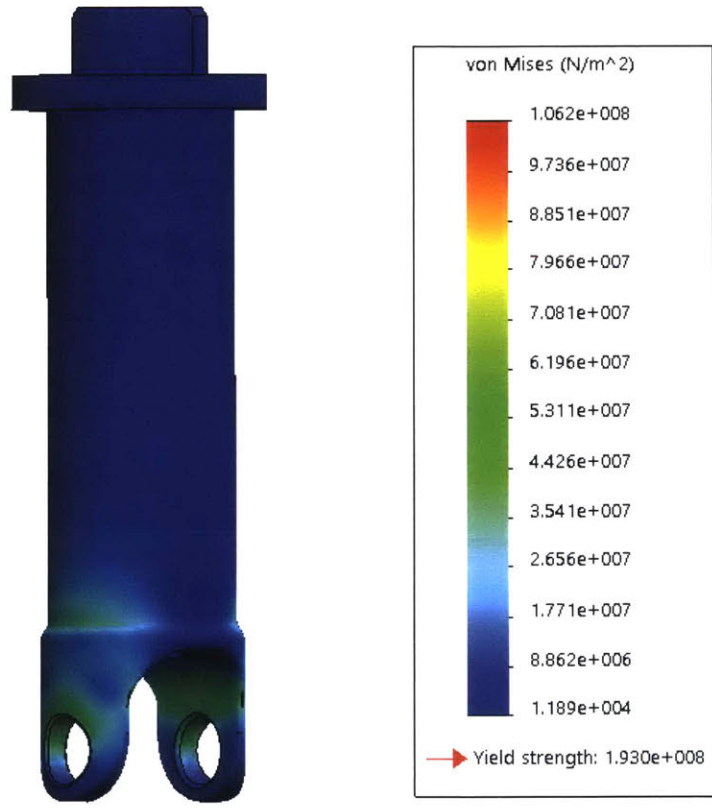


Figure 2-25: **Finite element analysis.** FEA was performed on all components. A representative result from the FEA performed on the ACME nut is shown here. The gradient of colors corresponds to level of stress in the component for the expected loading conditions.



# Chapter 3

## Results

### 3.1 Device Validation

The final ankle-foot prosthesis prototype was evaluated to determine if the device meets the design requirements. The original requirements as well as the final achieved values are presented in Table 3.1.

Table 3.1: **Final design specifications.** Initial requirements and resulting measured values for bionic climbing prosthesis.

Parameter	Requirement	Result
Range of Motion	Inversion/Eversion: +/- 20 degrees Plantar flexion/dorsiflexion: +/- 20 degrees	+/- 20.1 degrees +16.2/-18.7 degrees
Max Payload	100 kg	100+ kg
Free-space torque	1 Nm	> 1 Nm
Velocity	1 Rad/s	1 Rad/s
Mass	< 1400 g	1292 g
Build height	< 260 mm	260 mm
Battery life	> 2 hours	4 hours

#### 3.1.1 Mass

The mass distribution of the final system is outlined in table 3.2. The total mass is 1292 grams, which exceeds the design requirement for device mass. The mass of each component as well as total actuator and device mass is tabulated in Table 3.2.

Table 3.2: **System mass.** Final mass of each component, actuator assembly, and total device mass. The system weight is within the design specification, but can be further reduced by reducing the mass of the climbing foot or by using a smaller lithium polymer battery.

Component	Mass (g)	Quantity
Climbing foot	339	1
Lithium Polymer battery	78	1
Pyramid adapter	60	1
Pylon	57	1
Ankle joint	59	1
Bracket	52	1
Foot plate	32	1
Electronics housing	29	1
FlexSEA embedded system	22	1
Protective shell	16	1
Heat sink	7	1
U-joint block	2	5
Dowel pin 12 mm	1.5	5
Dowel pin 5 mm	0.5	10
Hardware	40	various
<b>Actuator</b>	<b>253</b>	2
Motor	66	2
Motor Housing	41	2
Bearing housing	30	2
Nut	27	2
Actuator housing	19	2
Futek LCM200	17	2
Lead screw	9	2
Load cell attachment	7	2
Angular contact bearing	7	4
Shaft coupler	5	2
Antibacklash nut	2	2
Motor mount	2	2
Bearing sleeve	0.3	2
Wave spring	0.7	2
<b>Total</b>	<b>1292</b>	

The mass of this device compares favorably to existing devices presented in Table 1.1. As shown in Table 3.2, the component with the largest mass is the custom climbing foot. Mass of the system could be reduced by changing the size or the material of the climbing foot. In future iterations a carbon fiber composite foot could

be designed to reduce device mass. The second heaviest component is the Lithium polymer battery. The selected battery is a 800 mAh 3 cell battery and during testing has lasted approximately 4 hours at a time. As our design requirement necessitates only a 2 hour battery life, this battery can be interchanged for a battery with a lower amp-hour rating, which will decrease the mass of the system.

### **3.1.2 Range of Motion**

Another important design requirement is the range of motion of the system. Range of motion of the system is evaluated by commanding the device throughout full range of motion of the actuators, and recording the actuator lengths at each position. Actuator encoder values are converted to joint angles, shown in Fig. 3-1.

The measured range of motion of the final system is 16.2 degrees dorsiflexion, -18.7 degrees plantar flexion, 20.1 degrees eversion, and -20.1 degrees inversion. The planter flexion and dorsiflexion values are slightly less than the specified design requirement. This is due to binding in the system that was occurring when the actuators reached their hard stops. In order to prevent this, the range of motion was mechanically limited and a software limit was added in the control system. In future iterations the range of motion can be increased by increasing the length of travel, or by preventing binding in the system by reducing friction between the components at the end of travel.

### **3.1.3 Control System**

The control system was analyzed to determine if the actuator bandwidth and accuracy are sufficient for neurally controlled biological movement. The actuator step response is analyzed by measuring the response time of the system to position targets for the position controller. Fig. 3-2 shows the position command target (dashed black) and the actuator response (blue). A position command was sent at a frequency of  $\frac{1}{3}$  Hz. The system reaches 90% of the target value in approximately 259 milliseconds. The speed of the step response is approximately 1 radian/second. This response time and

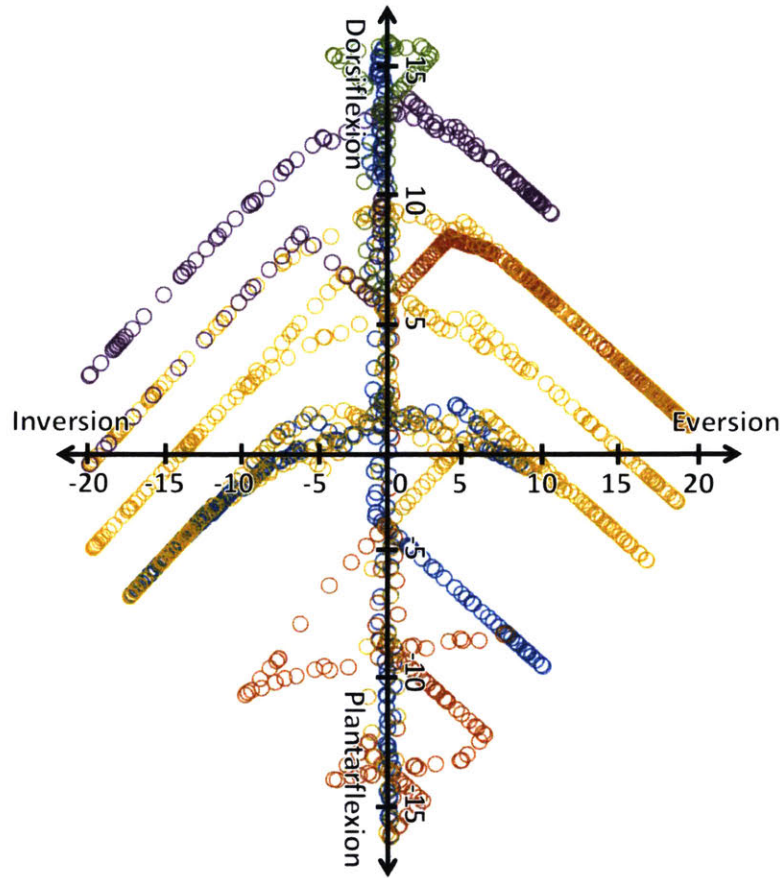


Figure 3-1: **Range of motion.** Ankle-foot prosthesis range of motion. Each point indicates the coordinates of a position reached, with the subtalar joint angle plotted on the x-axis and the ankle joint angle plotted on the y-axis.

actuator velocity meet the design requirements listed in Table 3.1.

### 3.1.4 Electronics

The performance of the electronics was analyzed by measuring motor current and motor voltage while moving the device at a speed of 1 radian/second (Fig. 3-3). The peak current is 3.2 amps during dorsiflexion and 3.0 amps during plantar flexion. Peak power is 15.5 watts, and power consumption of the electronics while the motors are not being driven is approximately 0.5 watts. This power consumption is higher than the expected power consumption calculated in Sec. 2.7.3, due to additional inefficiencies or increased friction in the system not accounted for in the initial calculation.

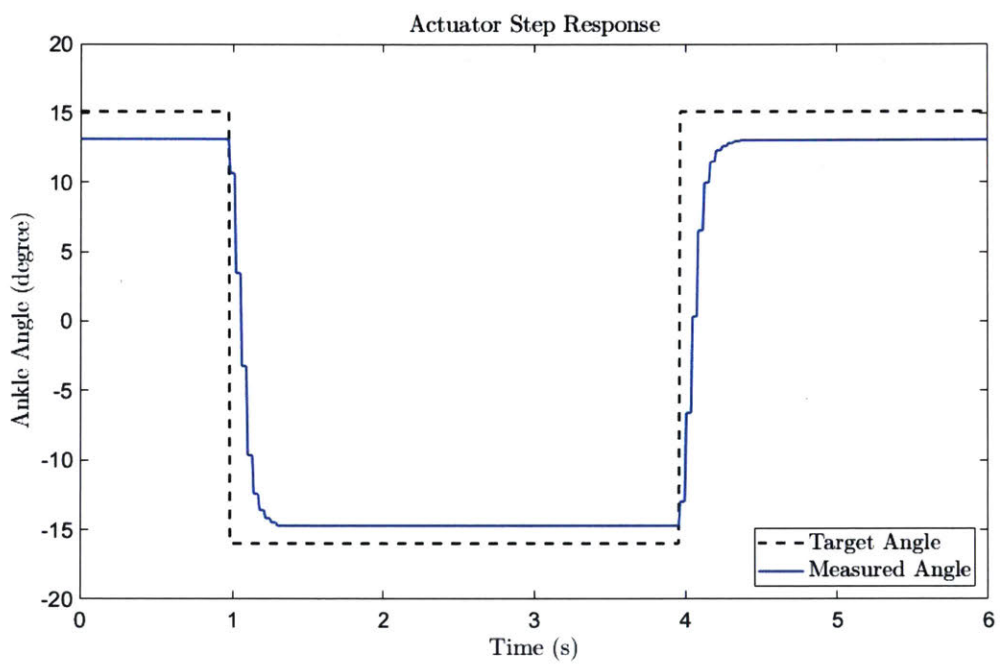


Figure 3-2: **Actuator step response.** Response time of position controller to step input (dashed black). Ankle angle (blue) 13 degrees dorsiflexion to -15 degrees plantar flexion, at a frequency of  $1/3$  Hz.

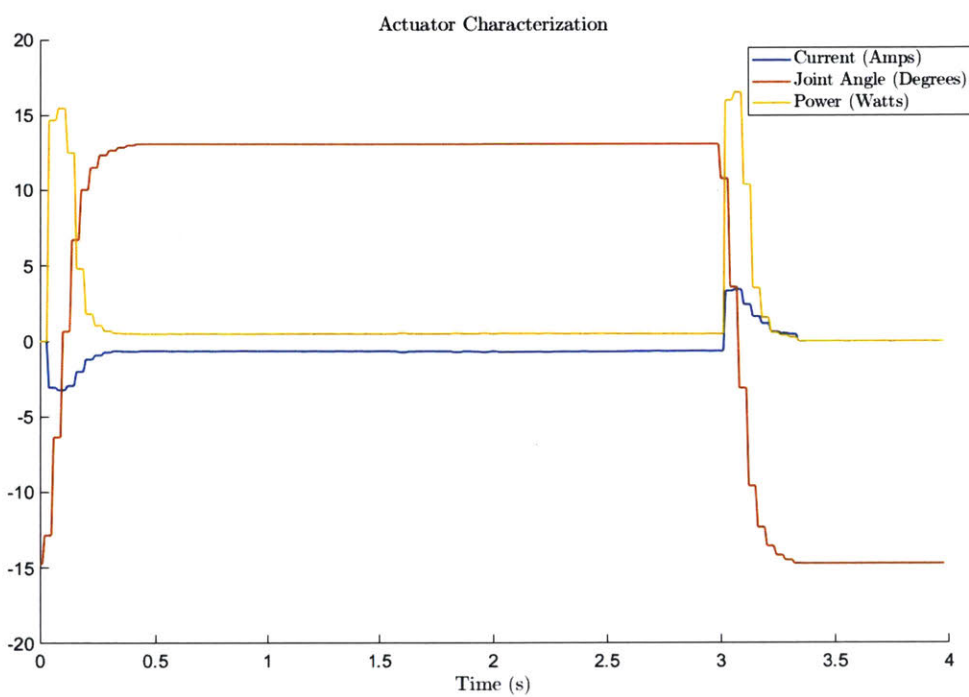


Figure 3-3: **Current, joint angle, and power through 4 cycles.** Motor current (amps), joint angle (degrees), and power (watts) averaged for two cycles of 13 degrees dorsiflexion to -15 degrees plantar flexion at a frequency of 1/3 Hz.

## 3.2 Clinical Evaluation

### 3.2.1 Experimental Design

To evaluate the presented hypotheses, a participant with a unilateral transtibial amputation performed rock climbing routes with his traditional passive rock climbing prosthesis and with the developed robotic device. This study was approved by the MIT Committee on the Use of Humans as Experimental Subjects, and written informed consent was obtained.

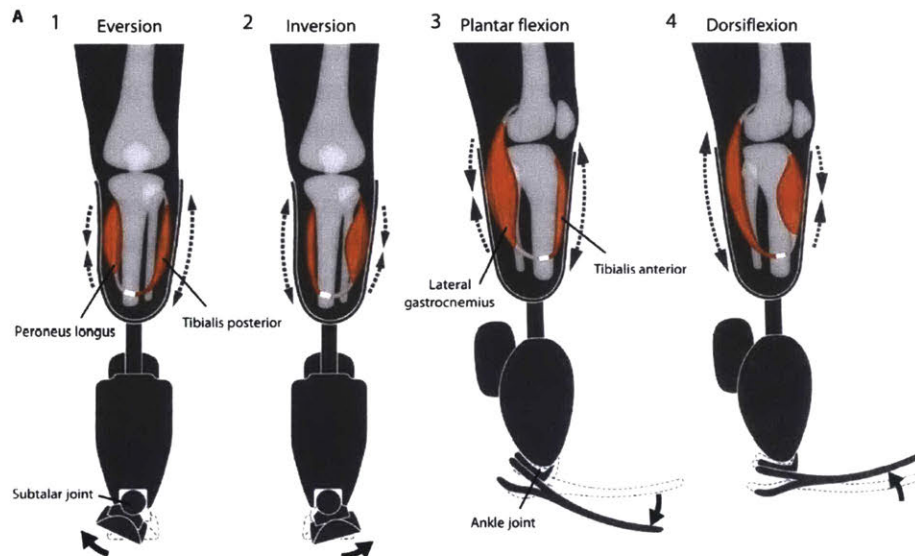


Figure 3-4: **Agonist-antagonist myoneural interface.** The subject for this study was a recipient of the agonist-antagonist myoneural interface amputation. This surgical technique preserves the agonist-antagonist relationship between muscles and maintains clear neural signals and proprioceptive feedback, allowing for robust control of robotic prostheses.

The participant with transtibial amputation (height: 172 cm, weight: 75 kg, age: 52 years, gender: male) is a trained, elite rock climber. The participant spent approximately seven hours training with the device prior to evaluation. The subject is a recipient of the agonist-antagonist myoneural interface amputation, with demonstrated improved efferent (from the central nervous system to the periphery) prosthetic control and afferent (from the periphery to the central nervous system) proprioceptive sensation [18]. Ten trials of a selected route in the climbing gym were used for



(a) Ankle goniometer.



(b) Knee goniometer.



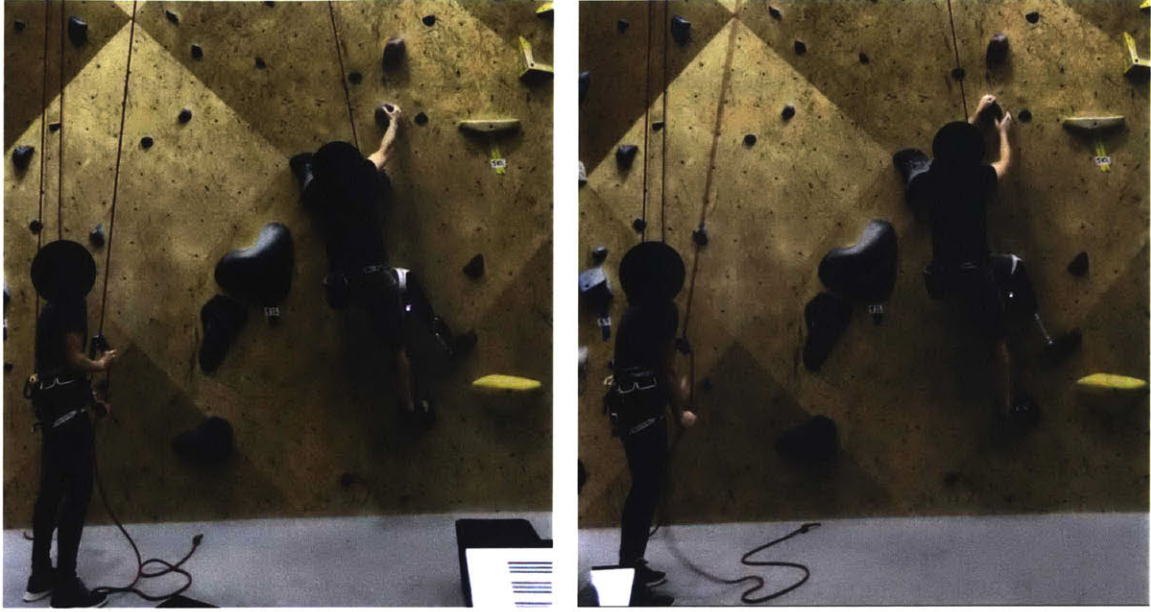
(c) Hip goniometer.

**Figure 3-5: EMG and goniometer sensor placement.** Ankle, knee, and hip goniometers placed on a control subject prior to evaluation. EMG muscle sensors are placed on the major muscle groups of the lower extremity.

**Table 3.3: Sensor placement during evaluation.** EMG sensor placement and goniometer sensor placement during human subject testing. Sensor placement was focused on the left leg as that is the side of amputation for the test subject.

	EMG Sensors	Goniometers
<b>Left Leg</b>	Tibialis anterior (TA)	Ankle
	Lateral gastrocnemius (LG)	Knee
	Peroneus longus (PL)	Hip
	Tibialis posterior (TP)	
	Rectus femoris (RF)	
	Hamstring (HAM)	
	Bulk abductors (ab)	
	Bulk adductors (ad)	
<b>Right Leg</b>	Tibialis anterior (TA)	
	Lateral gastrocnemius (LG)	
	Tibialis posterior (TP)	
	Rectus femoris (RF)	
	Hamstring (HAM)	
	Bulk abductors (ab)	
	Bulk adductors (ad)	

evaluation. The route was selected based on the difficulty level (5.10a) and variety of types of moves required. During the climbing session, biomechanical data was recorded using a wearable goniometer system, (Biometrics Ltd.), and muscle activation levels were recorded using surface electrodes (Delsys) (Table 3.3). The subject was asked to



(a) Trials with robotic prosthesis.

(b) Trials with passive prosthesis.

Figure 3-6: **Clinical evaluation.** Biomechanical data collection while climbing with powered ankle-foot prosthesis and passive rock climbing prosthesis. The subject climbed a 5.10a route in an indoor rock climbing gym while on a top rope belay.

Table 3.4: **Subjects for clinical evaluation.** Physical characteristics of test subject and control subjects. The control subjects were selected based on their similar height, weight, and climbing ability to the test subject.

Subject	Height	Weight	Age	Gender	Climbing Ability
Test Subject	172 cm	75 kg	52 years	M	5.11
Control 1	177.8 cm	76.2 kg	33 years	M	5.12
Control 2	167.6 cm	70.3 kg	58 years	M	5.11d
Control 3	175.3 cm	72.1 kg	39 years	M	5.12a

climb the first 20 feet of the selected route. Video was recorded to synchronize the recorded data with each move on the route. The experiments were performed with the bionic prosthesis as well as a passive prosthesis, in sets of 5 trials each of a random order. The trials were repeated with 3 control subjects with intact biological limbs of similar height, weight, gender, and climbing ability as the test subject. The control subjects were asked to climb the same route and were evaluated with the same sensor set as the test subject. The participants' physical characteristics and self reported climbing ability are listed in Table 3.4. Fig. 3-5 shows the sensor placement of the goniometers and EMG sensors on a control subject. Sensor placement (Table 3.3) was

determined in order to maximize data of interest collected for the available number of sensors. The left leg was the primary focus of data collection as that is the side of amputation for the test subject. Fig. 3-6 shows the experimental setup for the test subject climbing with the robotic prosthesis (Fig. 3-6a), and with a standard rock climbing prosthesis (Fig. 3-6b).

### 3.2.2 Results

Fig. 3-7 shows the joint angles of the test subject during the climbing study. Using the video and identifiable motions in the sensor data, the data was segmented into each individual climbing move for each trial. Fig. 3-7 show ankle, knee, and hip angles for the test subject during three moves on the climbing wall, from toe-off of the first hold to toe-off of the third hold. Average joint angles from the trials are shown for the active prosthesis (black) and the passive prosthesis (blue). Standard deviation is shown by the shading. The two most divergent outliers are excluded during data analysis. Table 3.5 shows the maximum average joint angles for each measures joint for the passive prosthesis and active prosthesis trials, as well as the individual control subjects and average control subjects. The maximum average plantar flexion achieved with the robotic prosthesis is -15.5 degrees, and maximum average dorsiflexion is 2.6 degrees. Maximum average eversion is 0.6 degrees, maximum average inversion is -4.5 degrees. The trials with the passive prosthesis show a fixed 0 degree ankle and subtalar joint. Knee angle also differs between the active prosthesis trials and passive

Table 3.5: **Maximum joint angles.** Maximum average joint angle for plantar flexion, dorsiflexion, inversion, eversion, knee flexion, hip flexion, abduction, and adduction while climbing.

	Passive	Powered	Control 1	Control 2	Control 3	Average Controls
Plantar Flexion	0°	-15.5°	-6.6°	-4.2°	-4.8°	-5.2°
Dorsiflexion	0°	2.6°	2.8°	27.8°	4.0°	11.5°
Inversion	0°	-4.5°	-21.3°	0°	-4.3°	-8.5°
Eversion	0°	0.6°	31.9°	41.0°	21.8°	31.6°
Knee Flexion	-60.9°	-42.9°	-96.2°	-102.0°	-54.2°	-84.1°
Hip Flexion	63.8°	63.9°	78.2°	71.8°	31.7°	60.6°
Abduction	-36.6°	-39.1°	-14.1°	-26.1°	-0.3°	-13.5°
Adduction	13.4°	17.5°	15.5°	33.6°	20.7°	23.3°

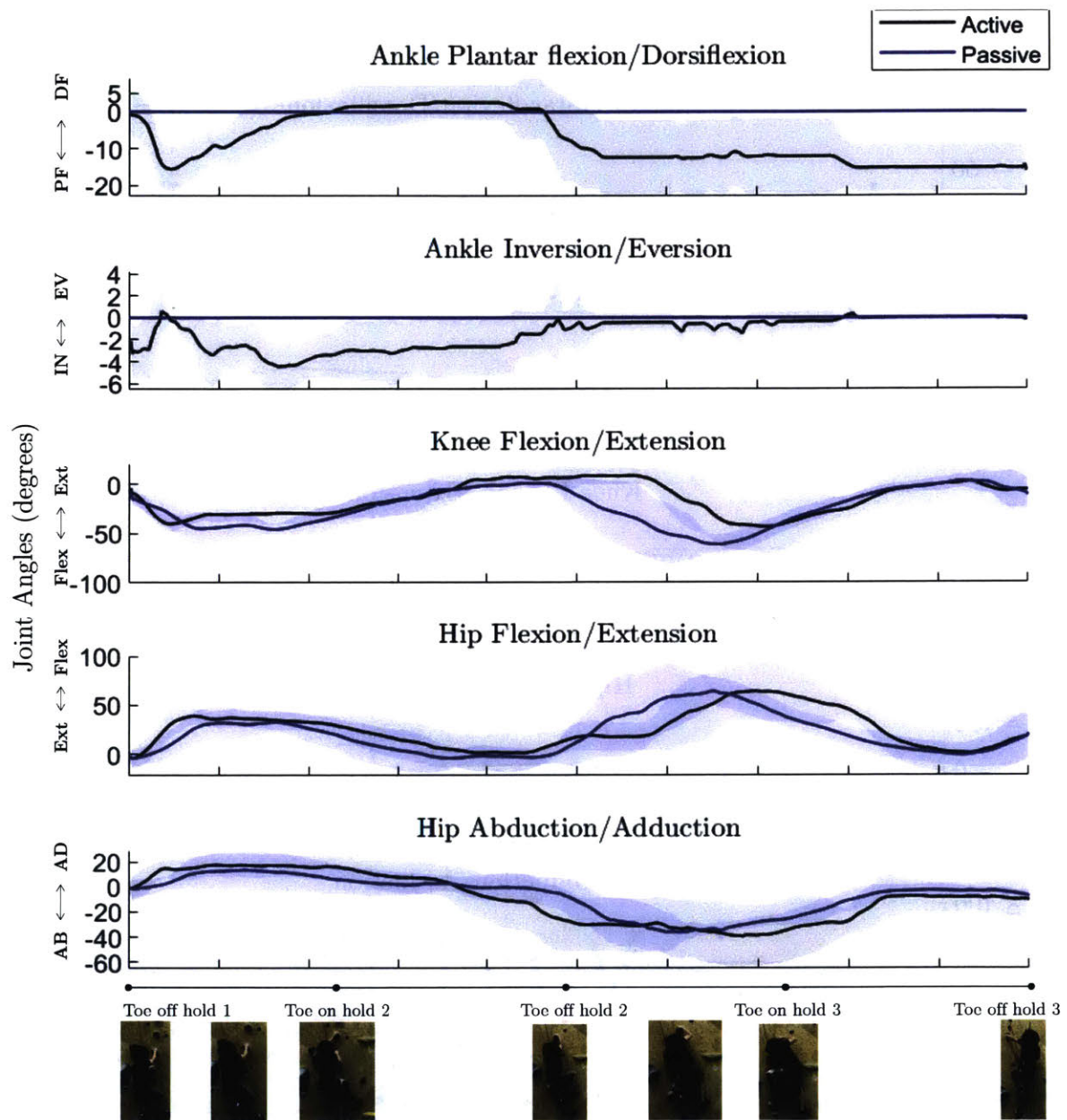


Figure 3-7: **Joint angles with passive prosthesis and powered prosthesis.** Joint angles of the ankle, knee, and hip during rock climbing with the passive prosthesis (blue), and the powered prosthesis (black). The trials are averaged and the standard deviation is shown in shading.

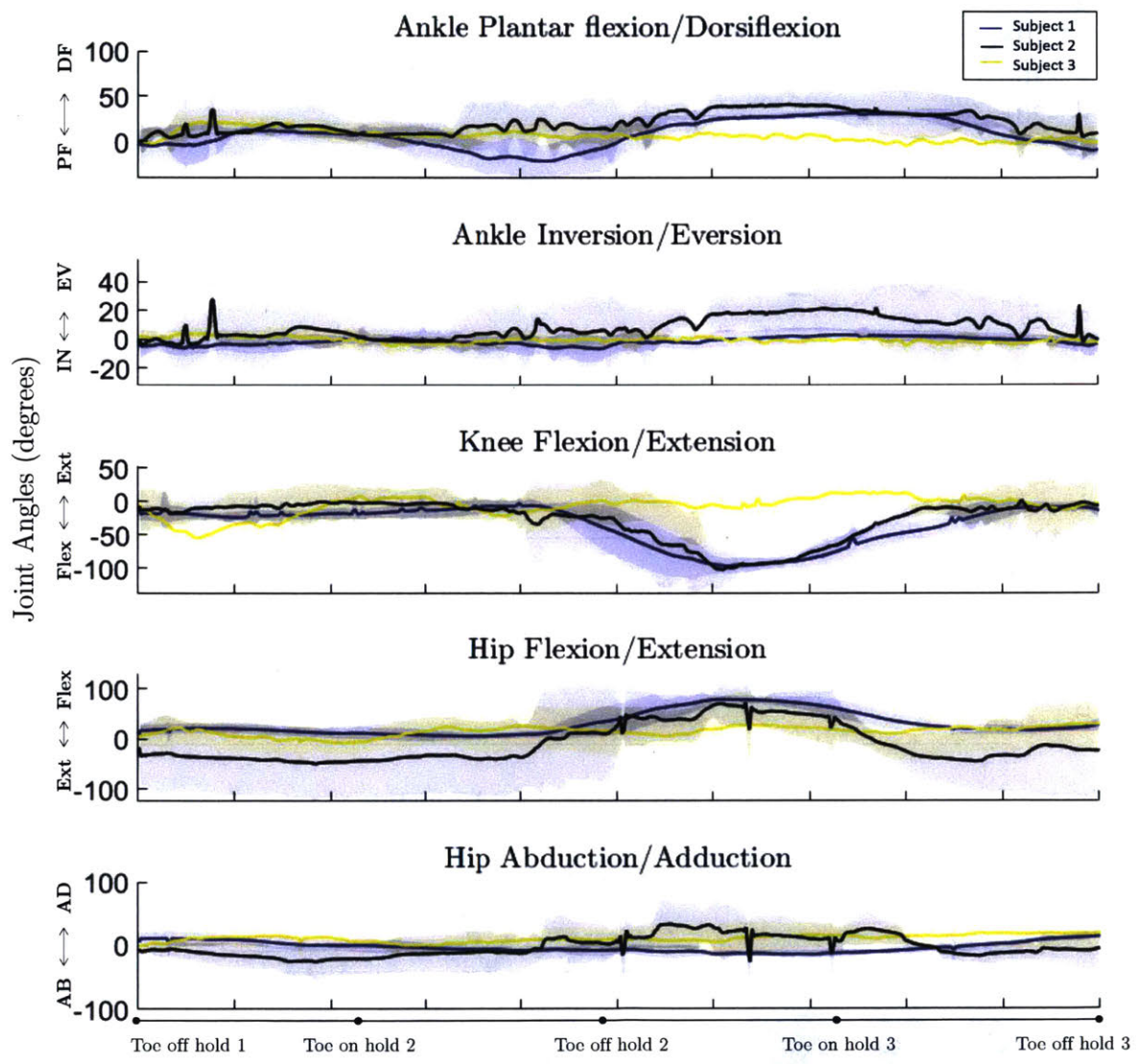


Figure 3-8: **Joint angles of control subjects.** Ankle, knee, and hip angles during rock climbing of Control 1 (blue), Control 2 (black), and Control 3 (yellow). The trials for each subject are averaged and the standard deviation is shown in shading.

prosthesis trials. Maximum knee flexion is lower while climbing with the powered prosthesis, -42.9 degrees compared to -60.9 degrees with the passive prosthesis. Hip flexion while climbing with the robotic prosthesis and passive prosthesis are reaches a maximum of 63.9 degrees, compared to a maximum of 63.8 degrees. Hip adduction reaches a maximum of 13.4 degrees with the passive prosthesis, compared with 17.5 degrees with the active prosthesis; hip abduction hits a maximum of -36.3 with the passive device compared with -39.1 degrees with the active prosthesis. Fig. 3-8 shows joint angles from the three control subjects during the climbing trials. The control subjects average maximum plantar flexion is -5.2 degrees, average dorsiflexion 11.5 degrees, average inversion -8.5 degrees, and average eversion 31.6 degrees. Knee flexion reaches an average maximum of -84.1 degrees, hip flexion 60.6 degrees, hip abduction -13.5 degrees, and hip adduction is 23.3 degrees.

### 3.3 Discussion

This chapter presents the results collected during device validation and human subject testing. Device validation shows that the prosthesis successfully achieves all design requirements. The design requirements for device mass, range of motion, control system response time, battery life, and ankle velocity are all achieved.

Human subject testing demonstrates that the subject with transtibial amputation utilizes both degrees of freedom of the rock climbing prosthesis while climbing. The subject is able to manipulate the position of the prosthesis in real time, effectively using the range of motion of the device to optimize foot placement on the holds.

The variability in climbing technique on the route selected makes a side by side comparison of joint angles between the control subjects and the test subject difficult. However, some trends emerge that demonstrate the benefit of the powered prosthesis over the passive prosthesis. Plantar flexion is greater while climbing with the powered prosthesis than the average controls joint angle. Plantar flexion of the robotic prosthesis is utilized the most, with an average of  $-15.5^\circ$  Dorsiflexion while climbing with the passive prosthesis is less than the average amongst all control subjects, but it is very

similar to control subjects 1 and 3 ( $2.6^\circ$  compared to  $2.8^\circ$  and  $4.0^\circ$ ). The inversion angle of  $-4.5^\circ$  achieved with the robotic prosthesis is also very similar to the  $-4.3^\circ$  inversion angle of control subject 3. Additionally, the narrow standard deviations achieved with the robotic ankle-foot prosthesis demonstrate the precise, repeatable control that the subject has via the neural inputs.

# Chapter 4

## Conclusions

### 4.1 Thesis Contributions

This thesis presents the first robotic ankle-foot prosthesis optimized for rock climbing. This ankle-foot prosthesis uses a novel non-backdrivable actuator approach to achieve more actuated degrees of freedom in a lower mass package than all existing powered prostheses. This device increases functionality substantially compared to commercially available passive rock climbing prostheses. This thesis presents initial results showing the utility of such a device for a person with transtibial amputation while rock climbing. This technology will increase accessibility of sports for people with amputation, helping improve physical and mental health as well as quality of life.

### 4.2 Future Work

Future work will include improving device packaging to create a waterproof system that may be used for outdoor climbing in all types weather. Additionally, the design can be improved to increase robustness, further decrease mass, and decrease build height to allow for people of all sizes and amputation levels to use the device.

Additional biomechanical studies will be performed to further explore the benefit that the device has on the biomechanics of people with transtibial amputation. Human subject data will be collected using full body motion capture to analyze the effect of

the robotic prosthesis on the full kinematic chain. The device will be tested while climbing on a wider variety of routes to determine what types of rock climbing moves the robotic ankle-foot prosthesis provides the most benefit for.

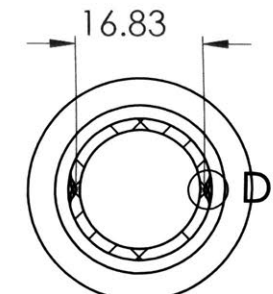
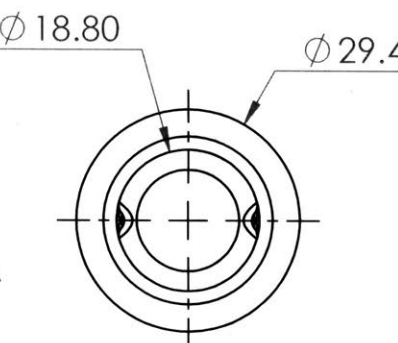
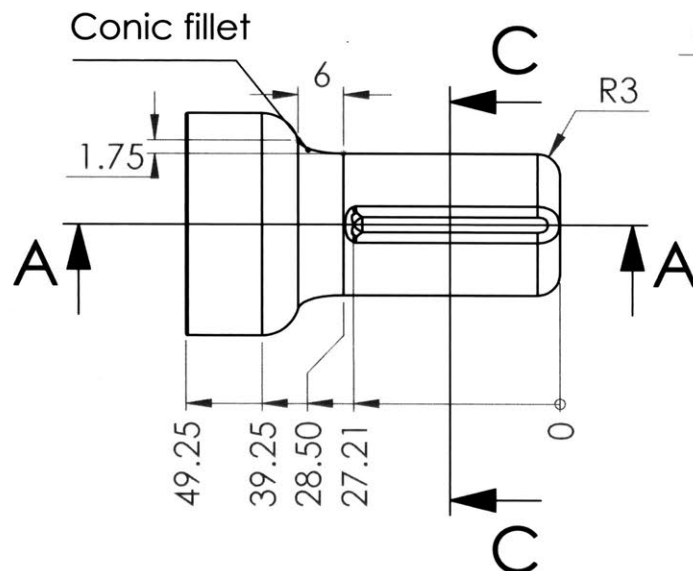
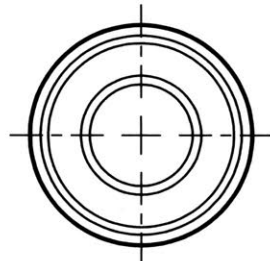
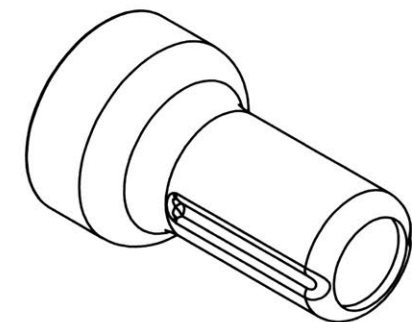
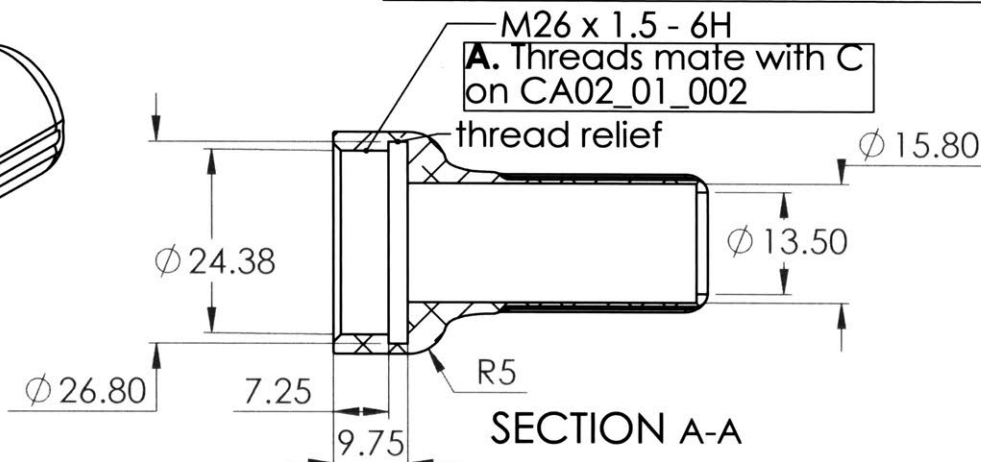
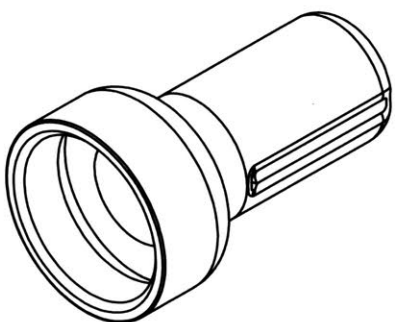
The prosthesis technology presented in this thesis has broad applications and could benefit any form of locomotion where actuated degrees of freedom are desired but a traditional powered prosthesis is too heavy. Future work includes adapting this technology to be used for terrain adaptation during hiking, safer stair ascent and descent during daily life, and swing phase toe clearance during walking. The novel design of a 2-degree-of-freedom prosthesis with a non-backdrivable transmission has the potential to increase access to robotic prostheses for people with lower limb amputation. This technology will provide a dramatic increase of function over a passive walking prosthesis at much lower cost and lower mass than a traditional powered prosthesis.

## Appendix A

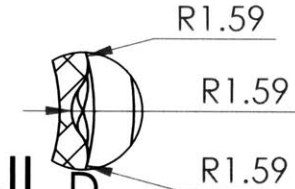
### Engineering Drawings

## REVISIONS

ZONE	REV.	DESCRIPTION	DATE	APPROVED
	B-02	Updated to indicate mating threads	1/26/2018	ER



SECTION C-C



DETAIL D

SCALE 3 : 1

## PROPRIETARY AND CONFIDENTIAL

THE INFORMATION CONTAINED IN THIS DRAWING IS THE SOLE PROPERTY OF MIT MEDIA LAB BIOMECHATRONICS. ANY REPRODUCTION IN PART OR AS A WHOLE WITHOUT THE WRITTEN PERMISSION OF MIT MEDIA LAB BIOMECHATRONICS IS PROHIBITED.

All dimensions are in mm and apply to finished (after plating) parts unless noted otherwise.

Break all sharp corners 0.25 max

Metric	[ Inch ]
.00 ± .2	.00 ± .01
.000 ± .1	.000 ± .005
.000 ± .02	.000 ± .001
.0000	+.0005 / -.00



biomechatronics

Massachusetts Institute of Technology  
Media Lab Biomechatronics  
75 Amherst St. Room E14-374N  
Cambridge, MA 02142  
+1 (617)680-0048  
emrogers@mit.edu

This Drawing is the property of MIT Media Lab Biomechatronics, and can not be reproduced without the expressed written consent of MIT Media Lab Biomechatronics.

CA02\_01\_003\_actuator housing

Material: 7075-T6 (SN)

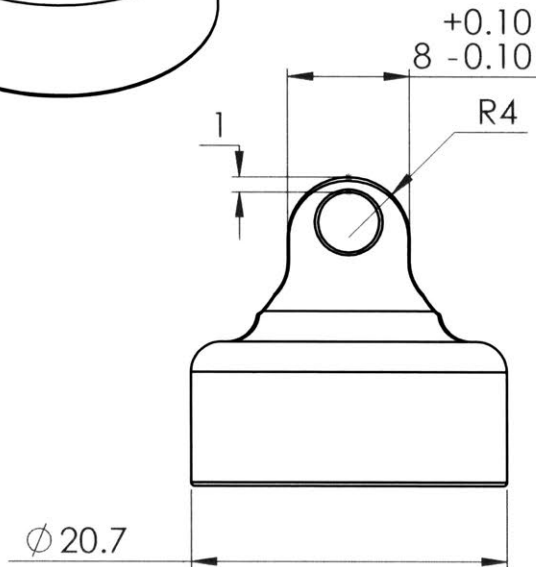
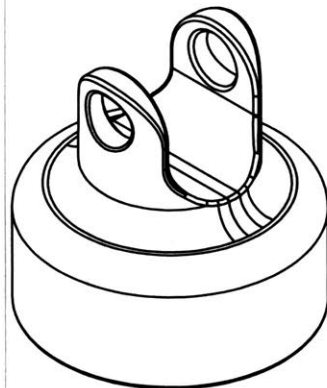
Finish: TUMBLE, CLEAR ANODIZE

1/26/2018

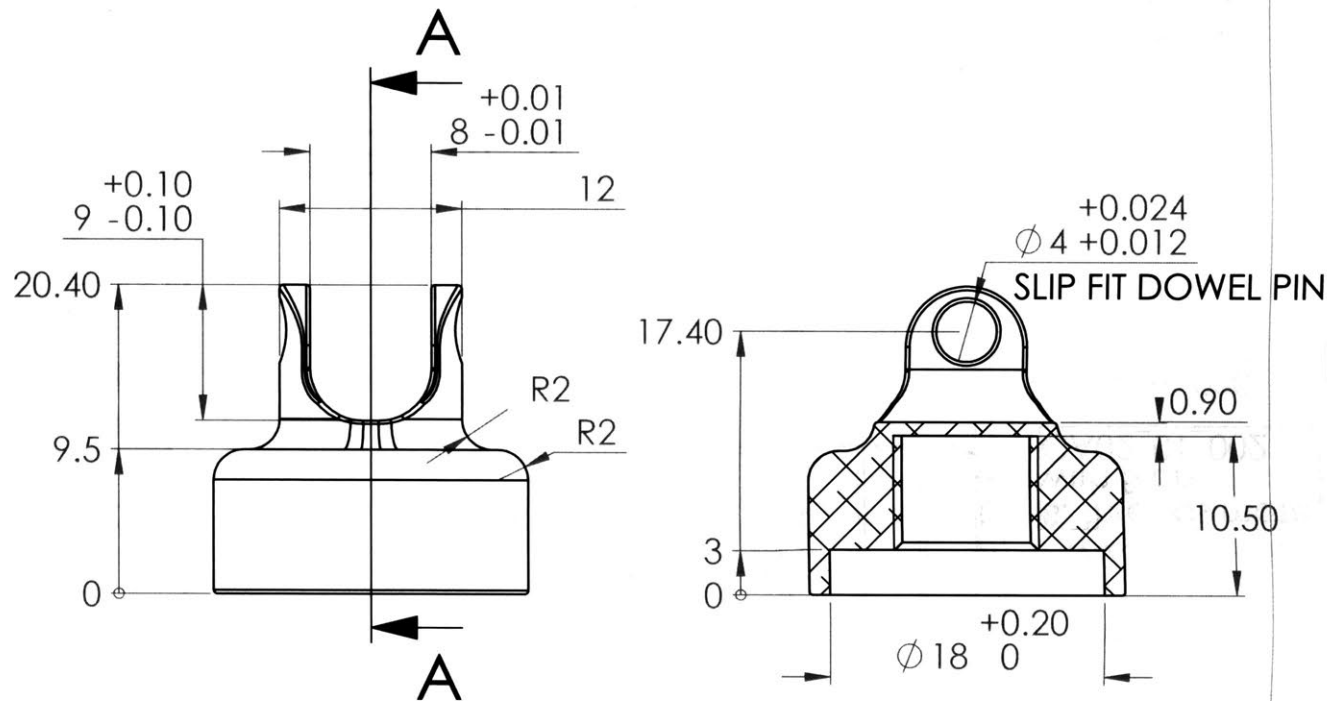
Scale 1:1

Sheet 1 of 1

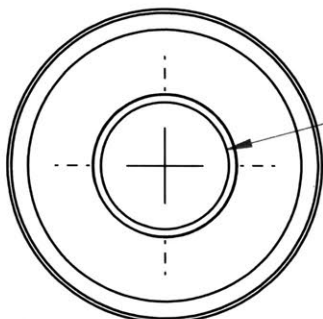
Rev - B-02



REV.		DESCRIPTION	DATE	APPROVED
ZONE				



SECTION A-A



All dimensions are in mm and apply to finished (after plating) parts unless noted otherwise.

Break all sharp corners 0.25 max

Metric	[ Inch ]
.0 ± .2	.0 ± .01
.000 ± .1	.00 ± .005
.0000 ± .02	.000 ± .001
.0000	/ .0005 / -0.0



biomechatronics

CA02\_01\_012\_load cell top

Massachusetts Institute of Technology  
Media Lab Biomechatronics  
75 Amherst St. Room E14-374N  
Cambridge, MA 02142  
+1 (617)680-0048  
emrogers@mit.edu

This Drawing is the property of  
MIT Media Lab Biomechatronics,  
and can not be reproduced  
without the expressed written  
consent of MIT Media Lab  
Biomechatronics.

1/28/2018

Scale 2:1

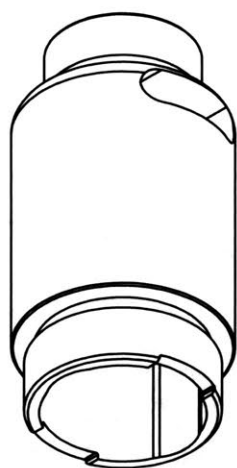
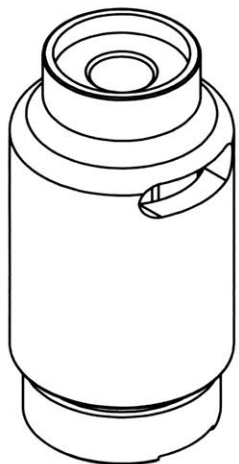
Sheet 1 of 1

Rev - B-01

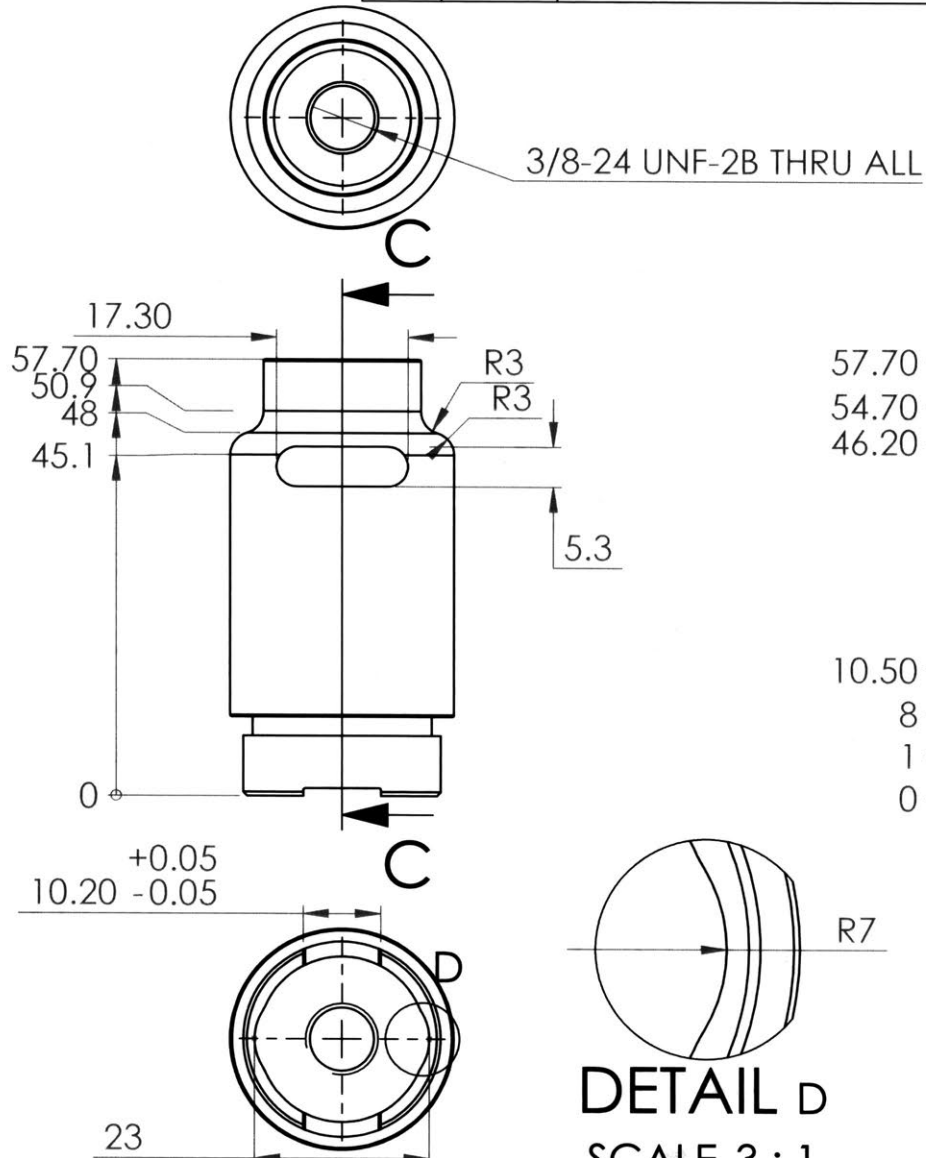
Material: See spreadsheet for material specification

Finish: TUMBLE, CLEAR ANODIZE

ZONE	REV.	DESCRIPTION	DATE	APPROVED
	B-02	Updated to indicate mating threads	1/26/2018	ER
	B-03	Revised dimensions of wire pass through slot	2/6/2018	ER



**PROPRIETARY AND CONFIDENTIAL**  
THE INFORMATION CONTAINED IN THIS DRAWING IS THE SOLE PROPERTY OF MIT MEDIA LAB BIOMECHATRONICS. ANY REPRODUCTION IN PART OR AS A WHOLE WITHOUT THE WRITTEN PERMISSION OF MIT MEDIA LAB BIOMECHATRONICS IS PROHIBITED.



**DETAIL D**  
SCALE 3 : 1

All dimensions are in mm and apply to finished (after plating) parts unless noted otherwise.  
Break all sharp corners 0.25 max

Metric	[ Inch ]
.00 ± .2	.0 ± .01
.00 ± .1	.00 ± .005
.000 ± .02	.000 ± .001
.0000 ± .0005	.0000 ± .0005



**CA02\_01\_000\_motor housing\_B03**

Material: 7075-T6 (SN)

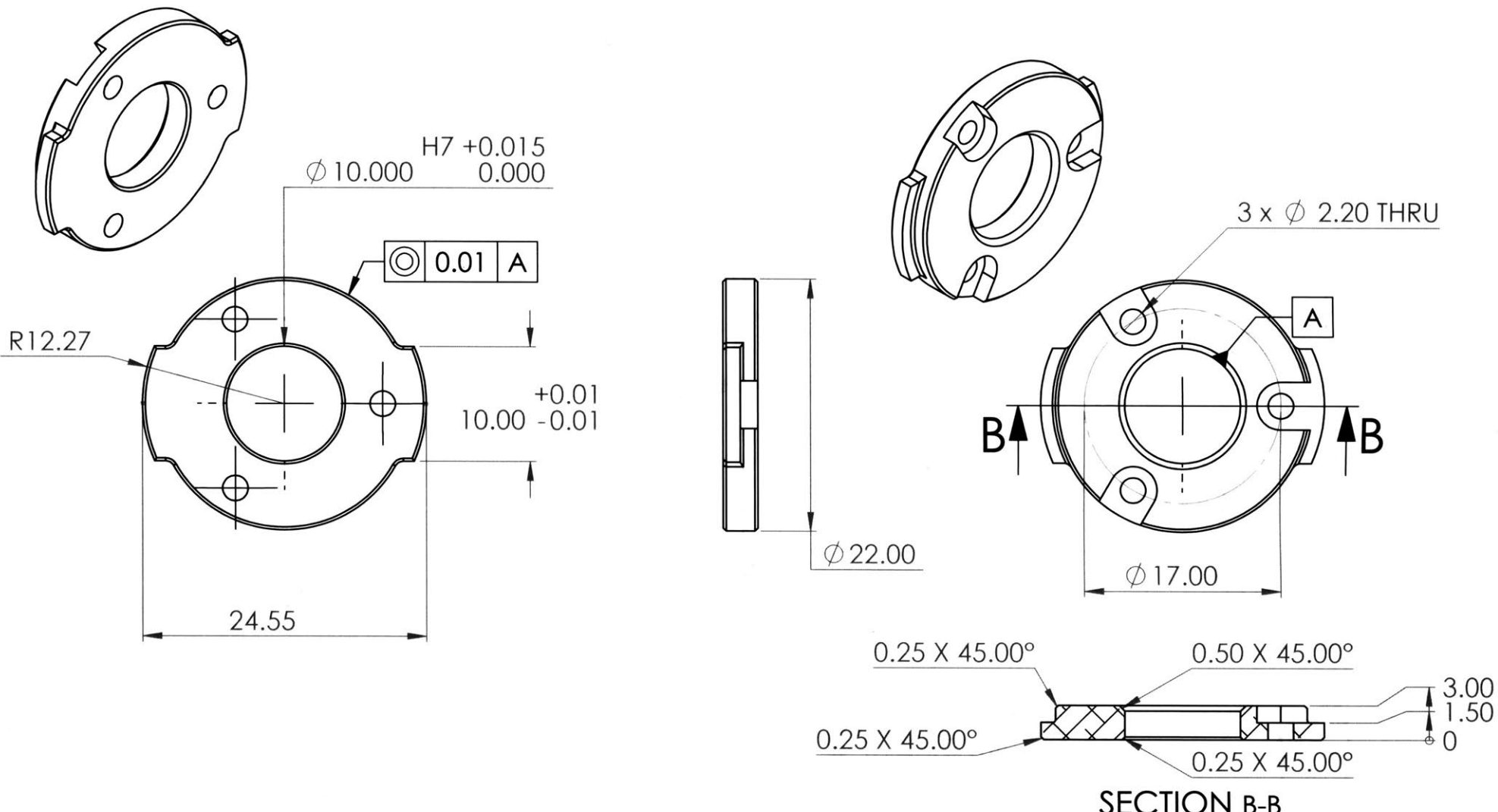
Finish: TUMBLE, CLEAR ANODIZE

Massachusetts Institute of Technology  
Media Lab Biomechatronics  
75 Amherst St. Room E14-374N  
Cambridge, MA 02142  
+1 (617)680-0048  
emrogers@mit.edu

This Drawing is the property of  
MIT Media Lab Biomechatronics,  
and can not be reproduced  
without the expressed written  
consent of MIT Media Lab  
Biomechatronics.

2/6/2018  
Scale 1:1  
Sheet 1 of 1  
Rev - B-03

REVISED		DESCRIPTION	DATE	APPROVED
ZONE	REV.			


**PROPRIETARY AND CONFIDENTIAL**

THE INFORMATION CONTAINED IN THIS DRAWING IS THE SOLE PROPERTY OF MIT MEDIA LAB BIOMECHATRONICS. ANY REPRODUCTION IN PART OR AS A WHOLE WITHOUT THE WRITTEN PERMISSION OF MIT MEDIA LAB BIOMECHATRONICS IS PROHIBITED.

All dimensions are in mm and apply to finished (after plating) parts unless noted otherwise.

Break all sharp corners 0.25 max

Metric	[ Inch ]
$.0 \pm .2$	$.0 \pm .01$
$.00 \pm .1$	$.00 \pm .005$
$.000 \pm .02$	$.000 \pm .001$
	$.0000 \pm .0005$
	$.0000 \pm .000$


**CA02\_01\_004\_motor mount**

Material: 7075-T6 (SN)

Massachusetts Institute of Technology  
Media Lab Biomechatronics  
75 Amherst St. Room E14-374N  
Cambridge, MA 02142  
+1 (617)680-0048  
[emrogers@mit.edu](mailto:emrogers@mit.edu)

This Drawing is the property of  
MIT Media Lab Biomechatronics,  
and can not be reproduced  
without the expressed written  
consent of MIT Media Lab  
Biomechatronics.

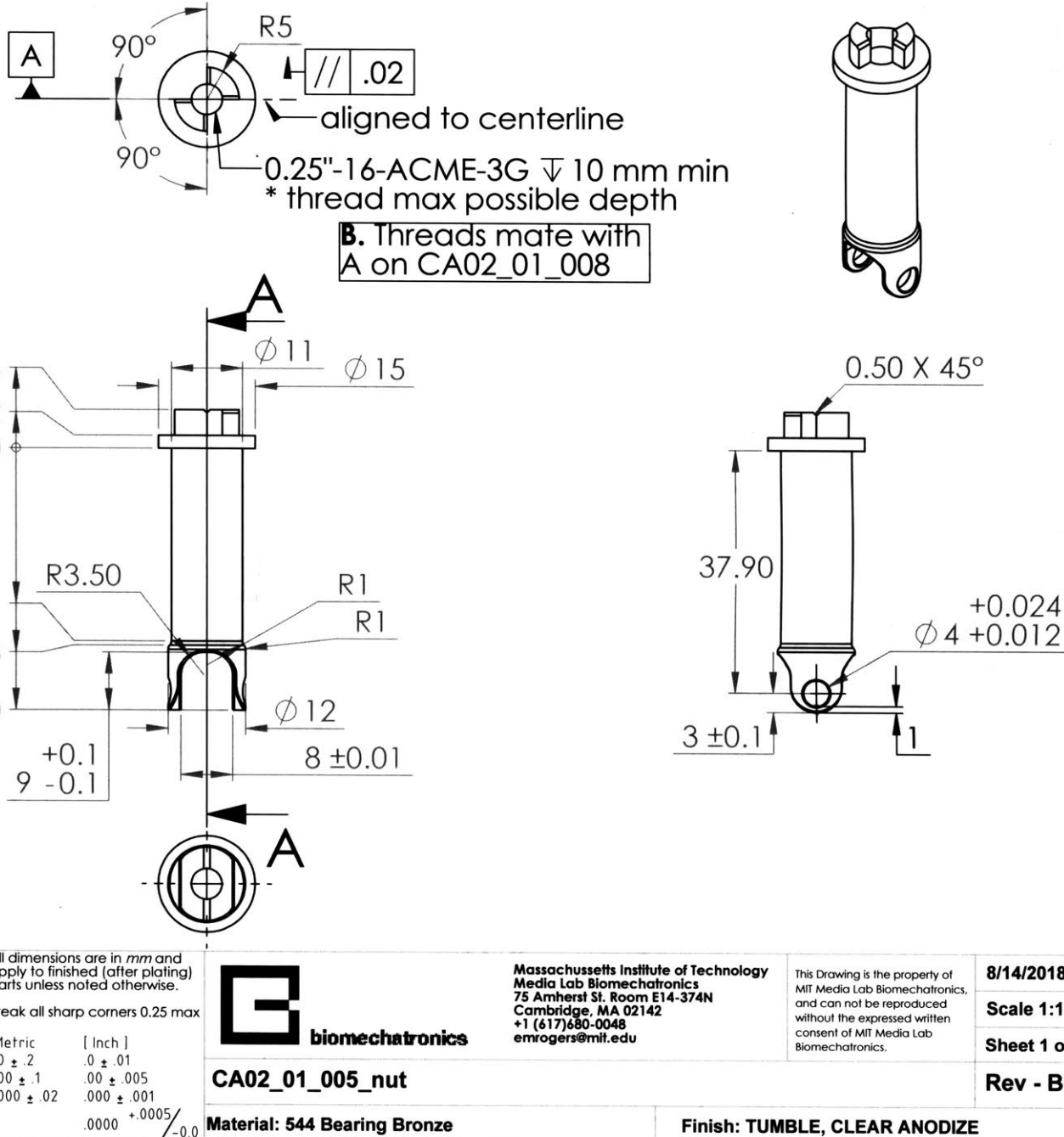
1/16/2018

Scale 2:1

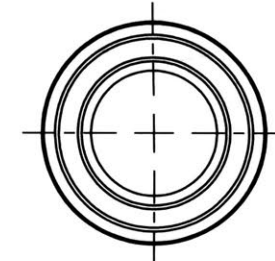
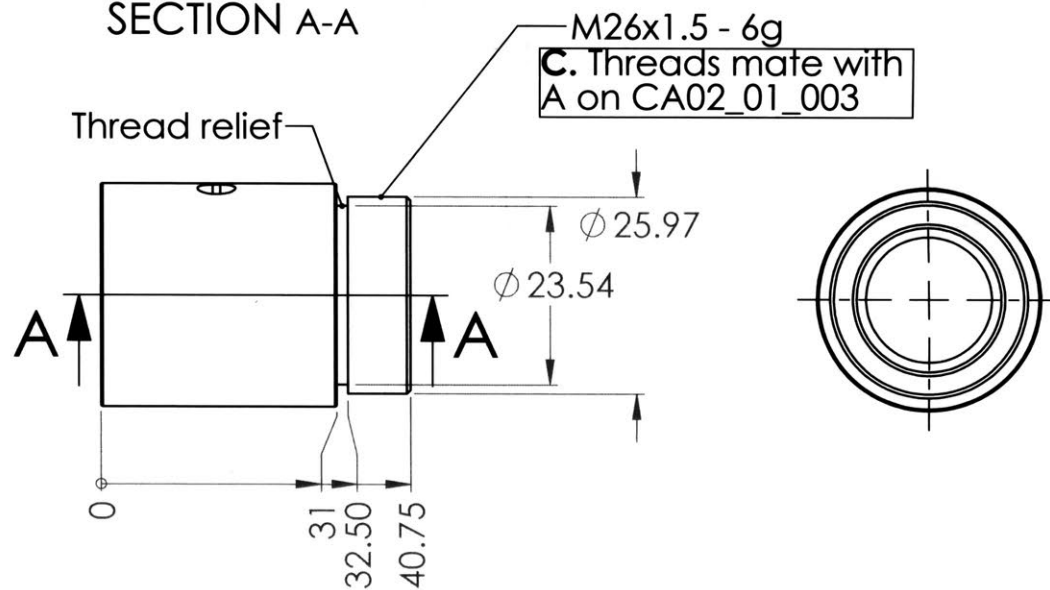
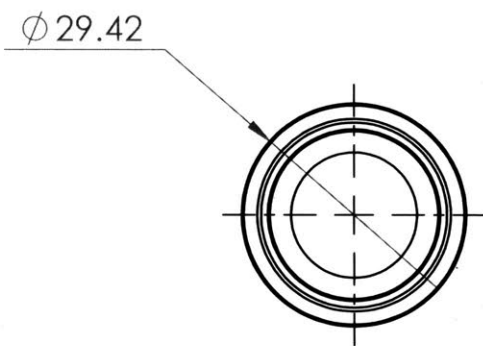
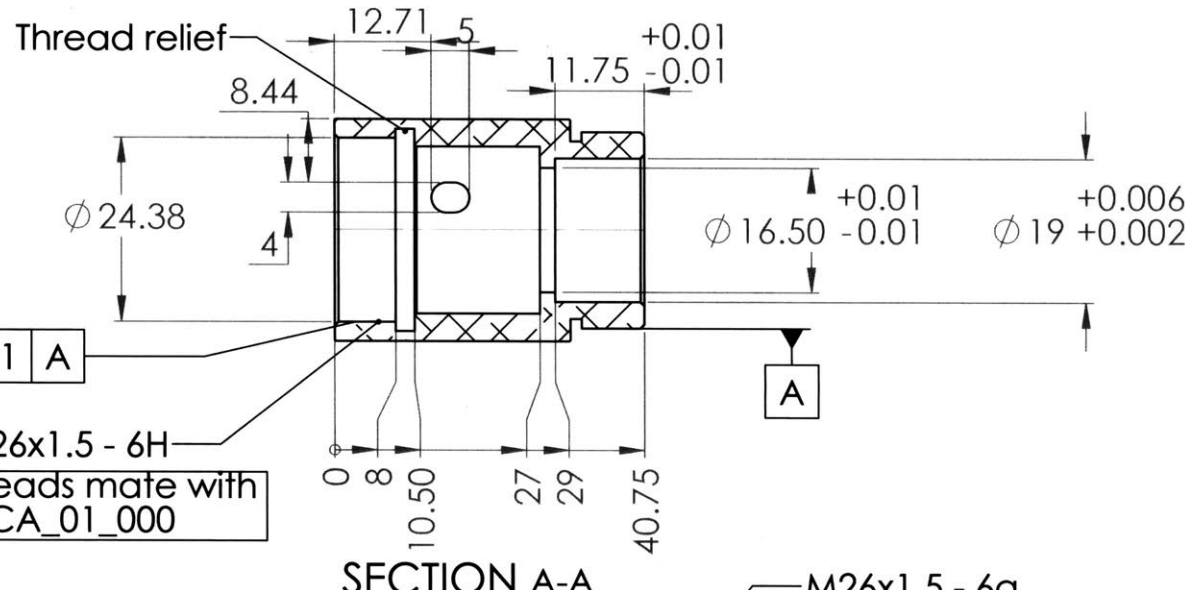
Sheet 1 of 1

Rev - B-01

ZONE	REV.	DESCRIPTION	DATE	APPROVED
	B-02	Updated to indicate mating threads	1/26/2018	ER
	B-03	Updated thread size and material	1/27/2018	ER
	B-04	Indicated end of part to thread	2/12/2018	ER



REVISED		DESCRIPTION	DATE	APPROVED
ZONE	REV.			
B-02		Updated to indicate mating threads	1/26/2018	ER



**PROPRIETARY AND CONFIDENTIAL**  
THE INFORMATION CONTAINED IN THIS DRAWING IS THE SOLE PROPERTY OF MIT MEDIA LAB BIOMECHATRONICS. ANY REPRODUCTION IN PART OR AS A WHOLE WITHOUT THE WRITTEN PERMISSION OF MIT MEDIA LAB BIOMECHATRONICS IS PROHIBITED.

All dimensions are in mm and apply to finished (after plating) parts unless noted otherwise.

Break all sharp corners 0.25 max

Metric	[ Inch ]
.00 ± .2	.00 ± .01
.00 ± .1	.00 ± .005
.000 ± .02	.000 ± .001
.0000 ± .0005 / -.00	



biomechatronics

Massachusetts Institute of Technology  
Media Lab Biomechatronics  
75 Amherst St. Room E14-374N  
Cambridge, MA 02142  
+1 (617)680-0048  
emrogers@mit.edu

This Drawing is the property of  
MIT Media Lab Biomechatronics,  
and can not be reproduced  
without the expressed written  
consent of MIT Media Lab  
Biomechatronics.

1/26/2018

Scale 1:1

Sheet 1 of 1

Rev - B-02

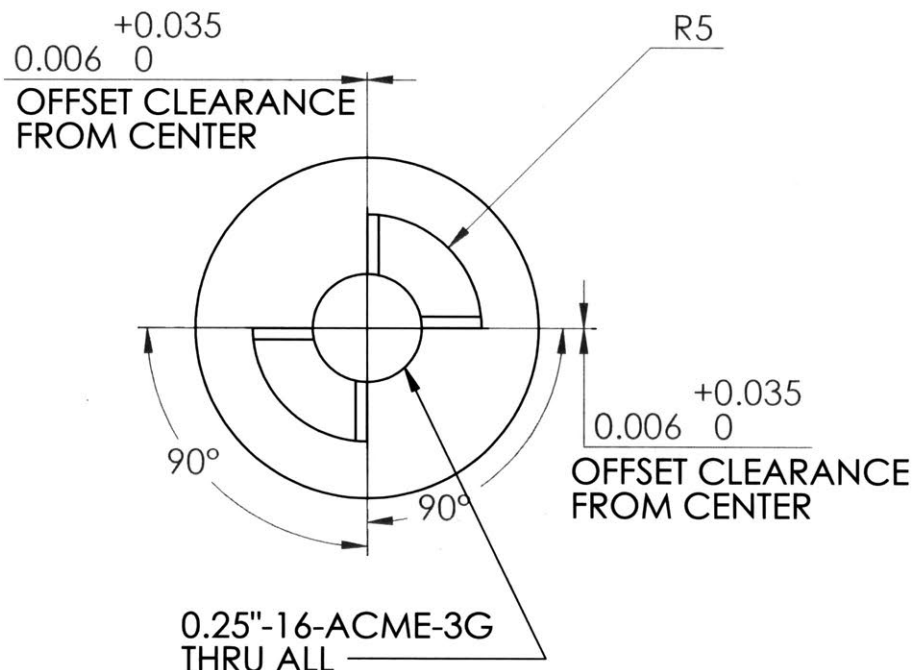
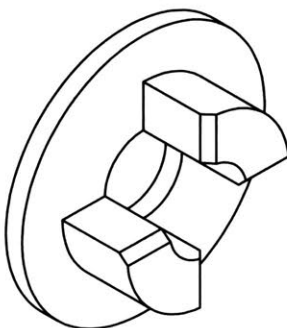
CA02\_01\_002\_bearing housing

Material: 7075-T6 (SN)

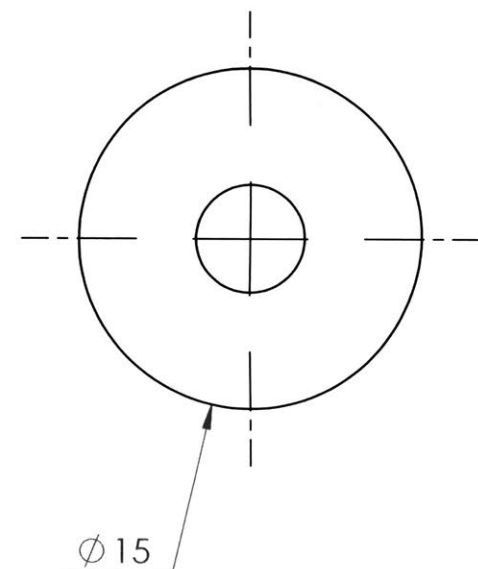
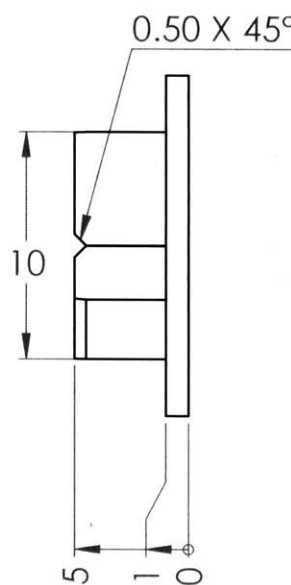
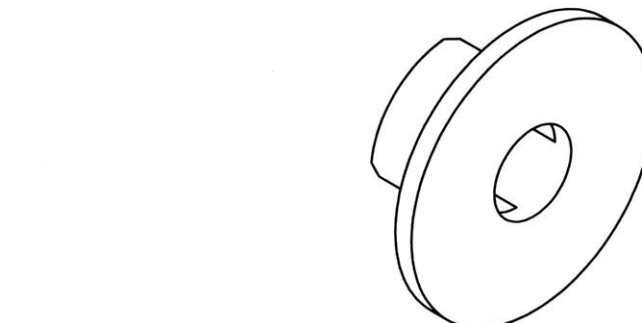
Finish: TUMBLE, CLEAR ANODIZE

## REVISIONS

ZONE	REV.	DESCRIPTION	DATE	APPROVED
	B-02	Updated to indicate mating threads	1/26/2018	ER
	B-03	Updated thread size and material	1/27/2018	ER



C. Threads mate with  
A on CA02\_01\_008



## PROPRIETARY AND CONFIDENTIAL

THE INFORMATION CONTAINED IN THIS DRAWING IS THE SOLE PROPERTY OF MIT MEDIA LAB BIOMECHATRONICS. ANY REPRODUCTION IN PART OR AS A WHOLE WITHOUT THE WRITTEN PERMISSION OF MIT MEDIA LAB BIOMECHATRONICS IS PROHIBITED.

All dimensions are in mm and apply to finished (after plating) parts unless noted otherwise.

Break all sharp corners 0.25 max

Metric	[Inch]
.0 ± .2	.0 ± .01
.00 ± .1	.00 ± .005
.000 ± .02	.000 ± .001
	.0000 ± .0005
	.0000 / -0.0



Massachusetts Institute of Technology  
Media Lab Biomechatronics  
75 Amherst St. Room E14-374N  
Cambridge, MA 02142  
+1 (617)680-0048  
emrogers@mit.edu

CA02\_01\_009\_antibacklash nut

Material: 544 Bearing Bronze

Finish: MACHINED, DEBURRED

This Drawing is the property of  
MIT Media Lab Biomechatronics,  
and can not be reproduced  
without the expressed written  
consent of MIT Media Lab  
Biomechatronics.

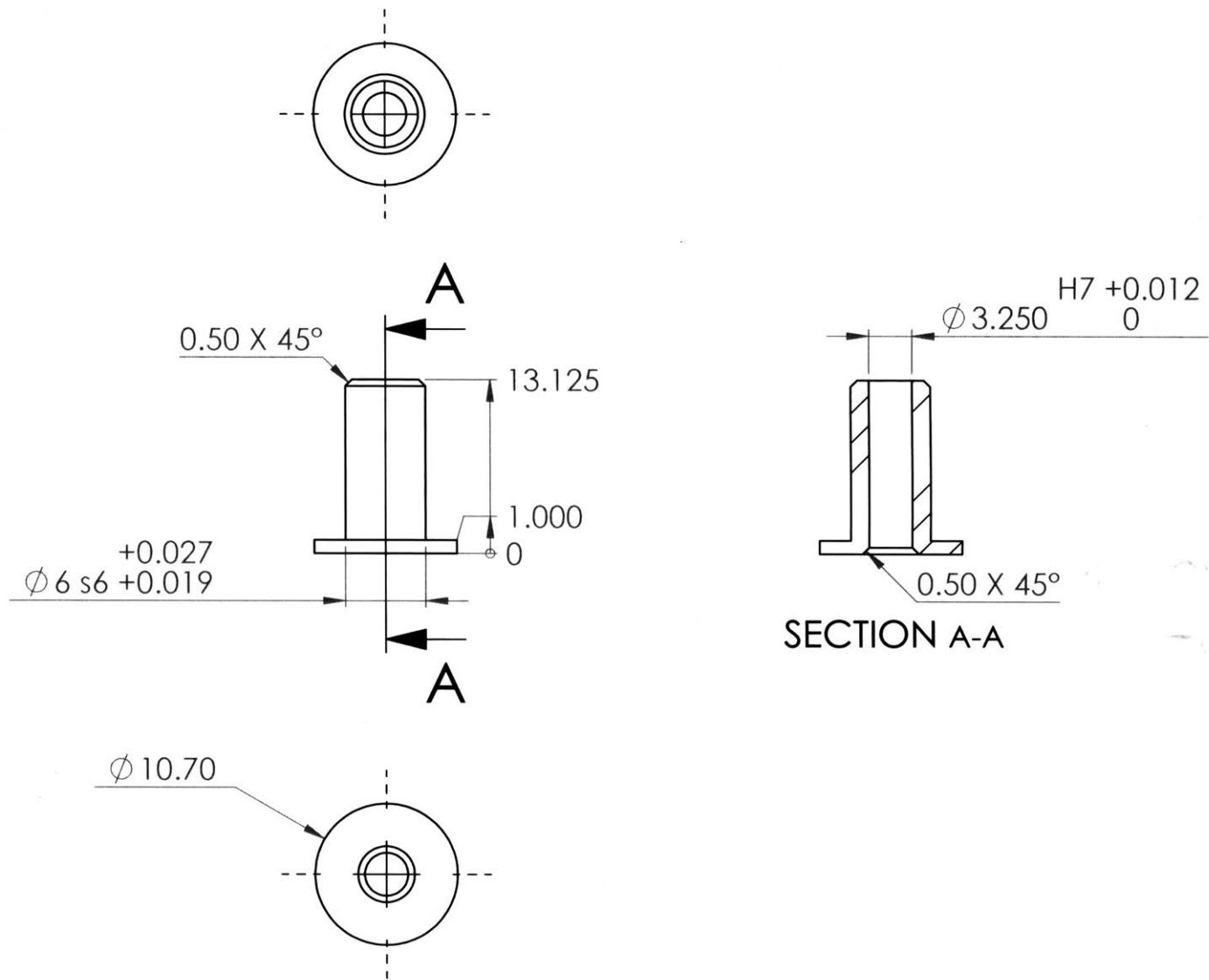
1/27/2018

Scale 3:1

Sheet 1 of 1

Rev - B-03

ZONE		REV.	REVISIONS	
			DESCRIPTION	DATE
				APPROVED



**PROPRIETARY AND CONFIDENTIAL**  
THE INFORMATION CONTAINED IN THIS DRAWING IS THE SOLE PROPERTY OF MIT MEDIA LAB BIOMECHATRONICS. ANY REPRODUCTION IN PART OR AS A WHOLE WITHOUT THE WRITTEN PERMISSION OF MIT MEDIA LAB BIOMECHATRONICS IS PROHIBITED.

All dimensions are in mm and apply to finished (after plating) parts unless noted otherwise.

Break all sharp corners 0.25 max

Metric	[ Inch ]
.00 ± .2	.0 ± .01
.00 ± .1	.00 ± .005
.000 ± .02	.000 ± .001
	.0000 ± .0005
	/ -0.0



**CA02\_01\_013\_bearing sleeve**

Material: AISI 303 Stainless Steel

Finish: MACHINED

Massachusetts Institute of Technology  
Media Lab Biomechatronics  
75 Amherst St. Room E14-374N  
Cambridge, MA 02142  
+1 (617)680-0048  
emrogers@mit.edu

This Drawing is the property of MIT Media Lab Biomechatronics, and can not be reproduced without the expressed written consent of MIT Media Lab Biomechatronics.

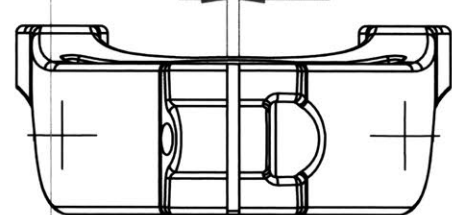
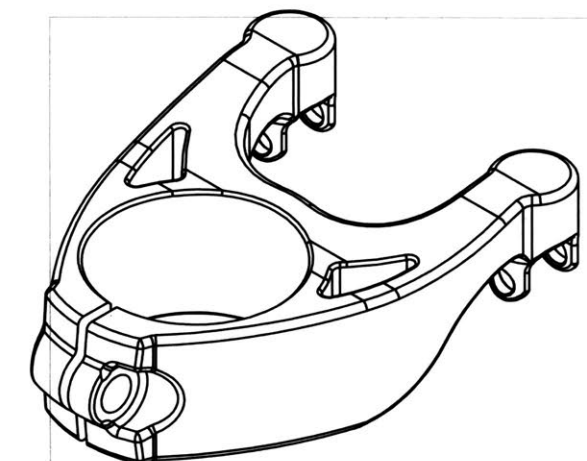
**1/16/2018**

**Scale 2:1**

**Sheet 1 of 1**

**Rev - B-01**

REV.		DESCRIPTION		DATE	APPROVED
ZONE					



1/32" corner radius end mill

### SECTION A-A

#### PROPRIETARY AND CONFIDENTIAL

THE INFORMATION CONTAINED IN THIS DRAWING IS THE SOLE PROPERTY OF MIT MEDIA LAB BIOMECHATRONICS. ANY REPRODUCTION IN PART OR AS A WHOLE WITHOUT THE WRITTEN PERMISSION OF MIT MEDIA LAB BIOMECHATRONICS IS PROHIBITED.

All dimensions are in mm and apply to finished (after plating) parts unless noted otherwise.

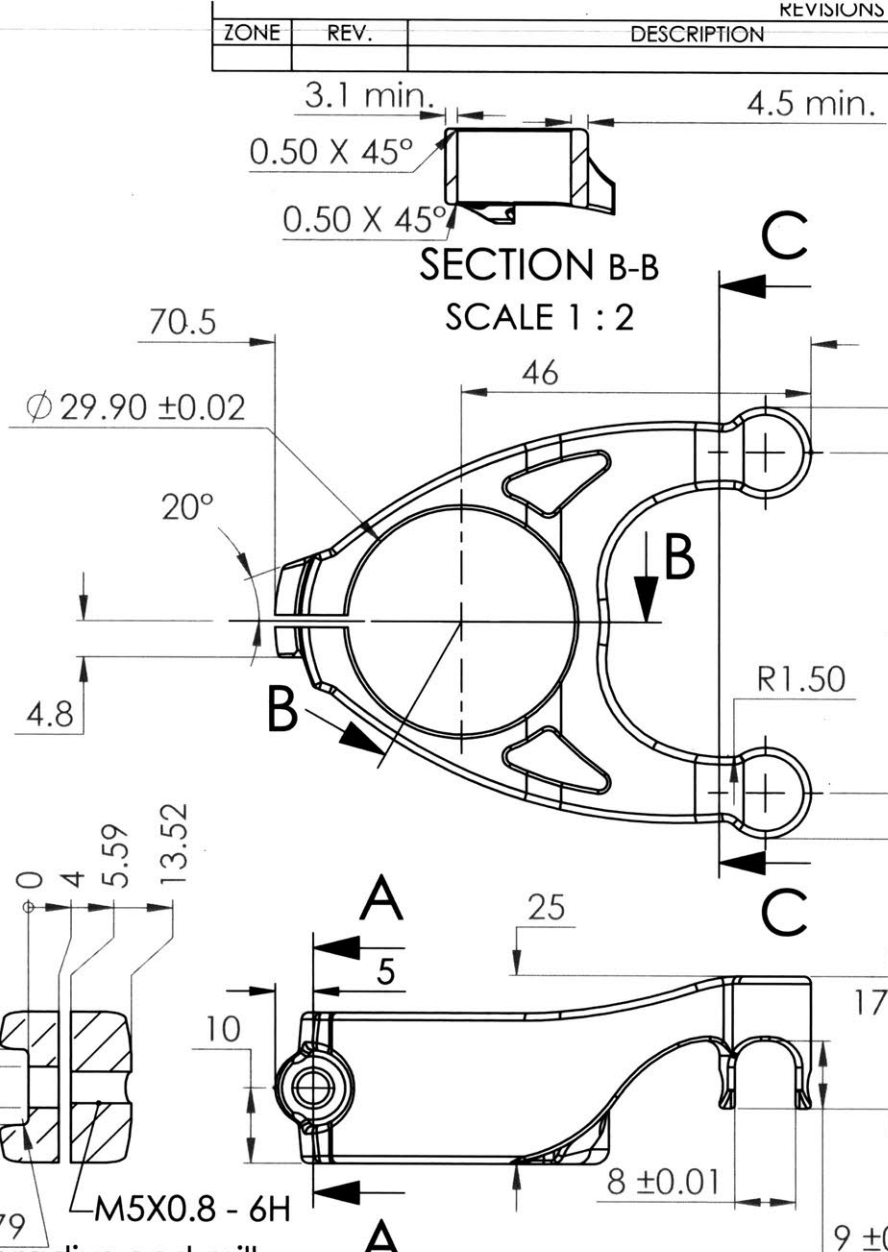
Break all sharp corners 0.25 min

Metric	[ Inch ]
.0 ± .2	.0 ± .01
.00 ± .1	.00 ± .005
.000 ± .02	.000 ± .001
.0000	+.0005 / -.00

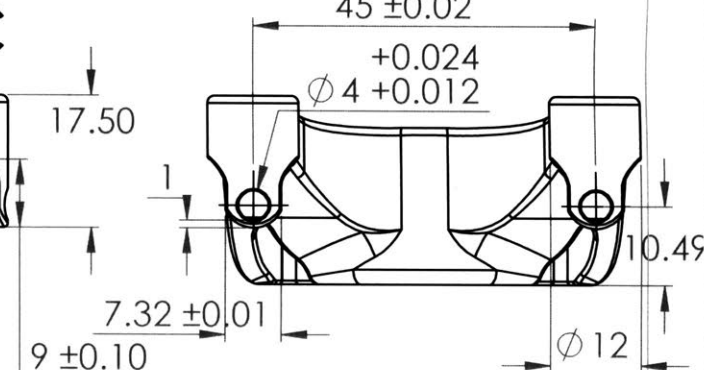


CA03\_01\_001\_bracket

Material: See spreadsheet for material specification | Finish: TUMBLE, CLEAR ANODIZE



SECTION C-C  
SCALE 1 : 2



Massachusetts Institute of Technology  
Media Lab Biomechatronics  
75 Amherst St, Room E14-374N  
Cambridge, MA 02142  
+1 (617)680-0048  
emrogers@mit.edu

This Drawing is the property of  
MIT Media Lab Biomechatronics,  
and can not be reproduced  
without the expressed written  
consent of MIT Media Lab  
Biomechatronics.

1/28/2018

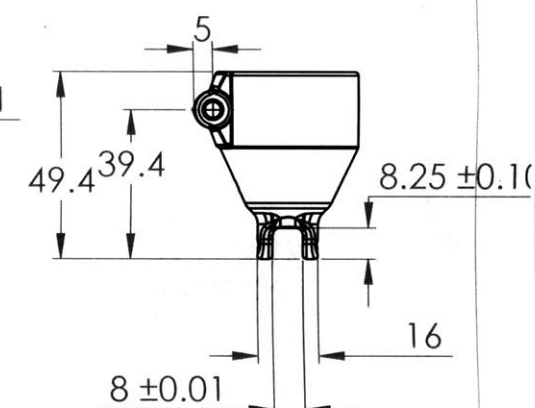
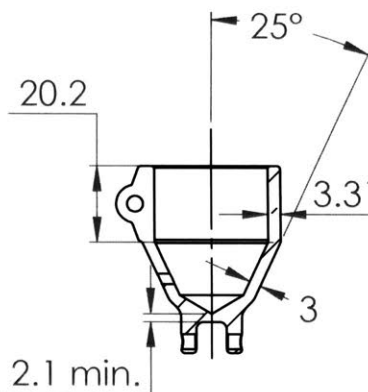
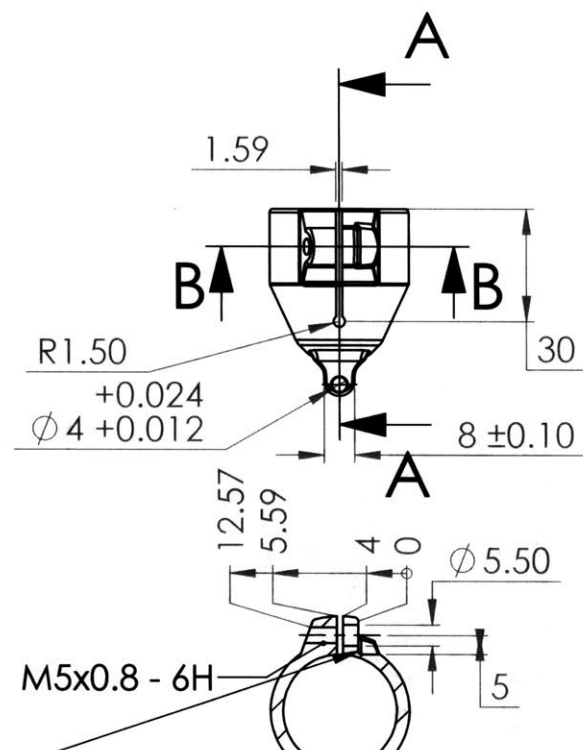
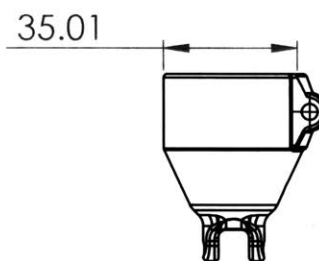
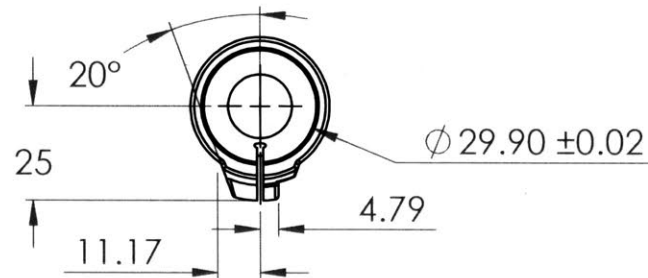
Scale 1:1

Sheet 1 of 1

Rev - A-01

## REVISIONS

ZONE	REV.	DESCRIPTION	DATE	APPROVED



1/32" corner radius end mill

SECTION B-B  
SCALE 1 : 2

## PROPRIETARY AND CONFIDENTIAL

THE INFORMATION CONTAINED IN THIS DRAWING IS THE SOLE PROPERTY OF MIT MEDIA LAB BIOMECHATRONICS. ANY REPRODUCTION IN PART OR AS A WHOLE WITHOUT THE WRITTEN PERMISSION OF MIT MEDIA LAB BIOMECHATRONICS IS PROHIBITED.

All dimensions are in mm and apply to finished (after plating) parts unless noted otherwise.

Break all sharp corners 0.25 min

Metric	[ Inch ]
.0 ± .2	.0 ± .01
.00 ± .1	.00 ± .005
.000 ± .02	.000 ± .001
	.0000 ± .0005 / -.00



biomechatronics

Massachusetts Institute of Technology  
Media Lab Biomechatronics  
75 Amherst St, Room E14-374N  
Cambridge, MA 02142  
+1 (617)680-0048  
emrogers@mit.edu

This Drawing is the property of  
MIT Media Lab Biomechatronics,  
and can not be reproduced  
without the expressed written  
consent of MIT Media Lab  
Biomechatronics.

1/28/2018

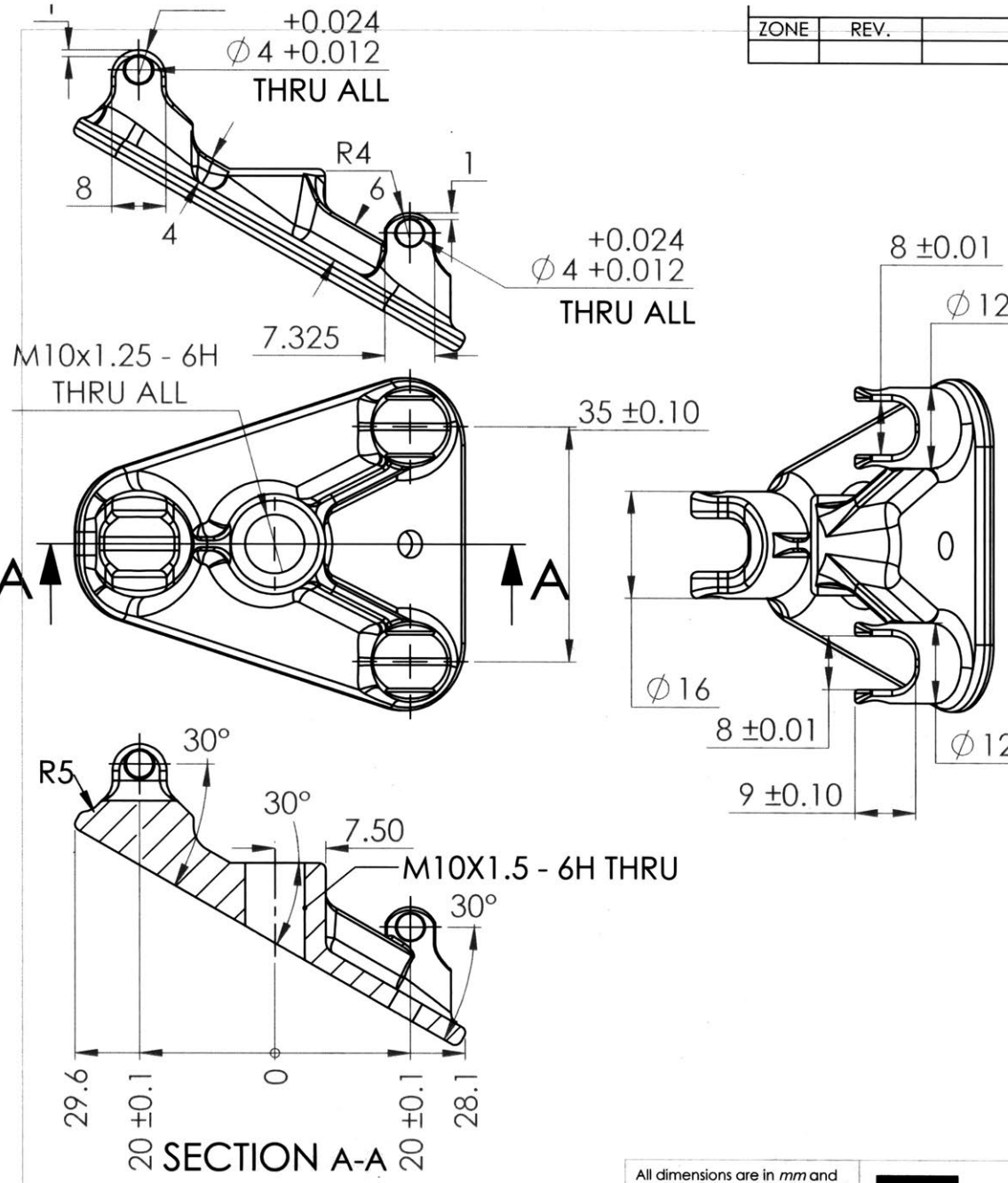
Scale 1:2

Sheet 1 of 1

Rev - A-01

CA03\_01\_002\_ankle joint

Material: See spreadsheet for material specification | Finish: TUMBLE, CLEAR ANODIZE



## SECTION A-A

### PROPRIETARY AND CONFIDENTIAL

THE INFORMATION CONTAINED IN THIS DRAWING IS THE SOLE PROPERTY OF MIT MEDIA LAB BIOMECHATRONICS. ANY REPRODUCTION IN PART OR AS A WHOLE WITHOUT THE WRITTEN PERMISSION OF MIT MEDIA LAB BIOMECHATRONICS IS PROHIBITED.

All dimensions are in mm and apply to finished (after plating) parts unless noted otherwise.

Break all sharp corners 0.25 min

Metric	[ Inch ]
.00 ± .2	.0 ± .01
.00 ± .1	.00 ± .005
.000 ± .02	.000 ± .001
.0000	+.0005 / -.00

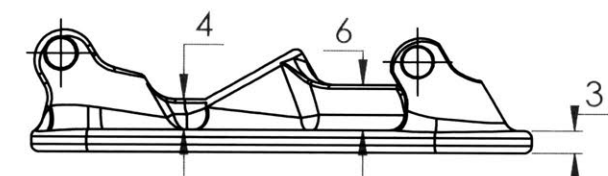
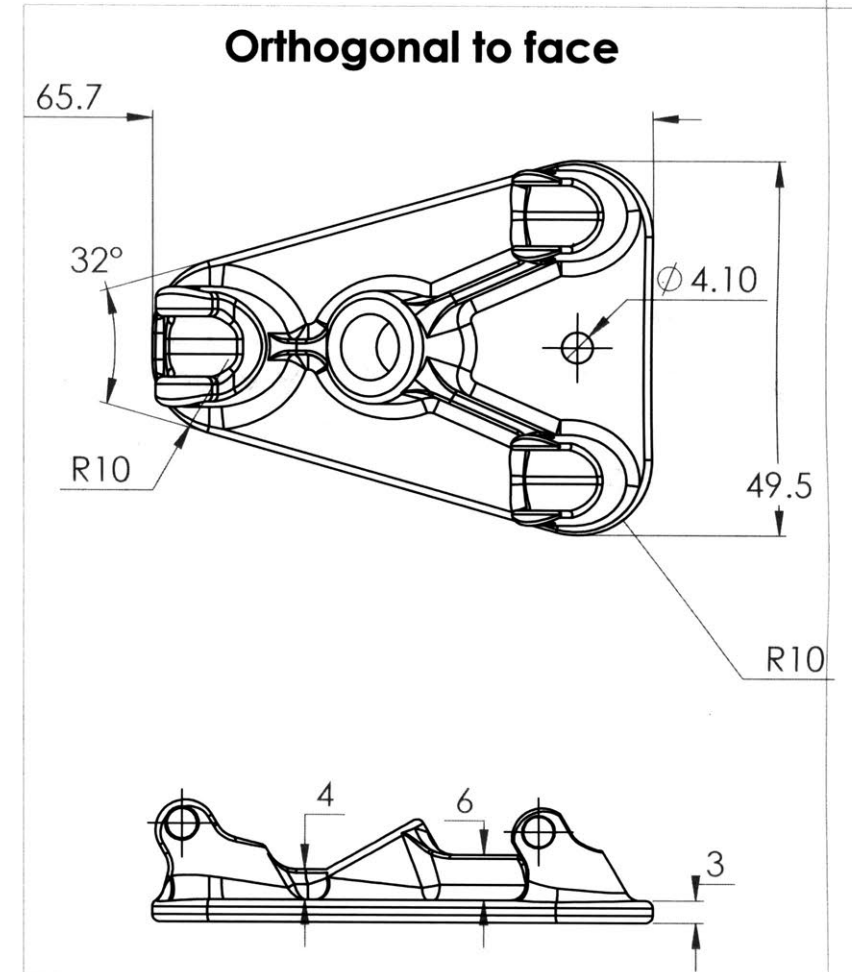


CA03\_01\_003\_foot plate

Material: See spreadsheet for material specification Finish: TUMBLE, CLEAR ANODIZE

ZONE	REV.	DESCRIPTION	DATE	APPROVED

## Orthogonal to face



Massachusetts Institute of Technology

Media Lab Biomechatronics  
75 Amherst St, Room E14-374N  
Cambridge, MA 02142  
+1 (617)680-0048  
emrogers@mit.edu

This Drawing is the property of MIT Media Lab Biomechatronics, and can not be reproduced without the expressed written consent of MIT Media Lab Biomechatronics.

1/28/2018

Scale 1:1

Sheet 1 of 1

Rev - A-01

# Bibliography

- [1] S.K. Au, J. Weber, and H. Herr. Powered Ankle–Foot Prosthesis Improves Walking Metabolic Economy. *IEEE Transactions on Robotics*, 25(1):51–66, February 2009.
- [2] Melanie Couture, Chantal D. Caron, and Johanne Desrosiers. Leisure activities following a lower limb amputation. *DISABILITY AND REHABILITATION*, 32(1):57–64, 2010.
- [3] Mihai Bragaru, C. P. van Wilgen, Jan H. B. Geertzen, Suzette G. J. B. Ruijs, Pieter U. Dijkstra, and Rienk Dekker. Barriers and Facilitators of Participation in Sports: A Qualitative Study on Dutch Individuals with Lower Limb Amputation. *PLoS ONE*, 8(3):e59881, March 2013.
- [4] Arthur Jason De Luigi and Rory A. Cooper. Adaptive sports technology and biomechanics: prosthetics. *PM & R: the journal of injury, function, and rehabilitation*, 6(8 Suppl):S40–57, August 2014.
- [5] The Foot & Ankle, December 2015.
- [6] Christopher John Low. *Biomechanics of rock climbing technique*. phd, University of Leeds, June 2005.
- [7] TRS Climbing. El Dorado Z-Axis Foot.
- [8] Evolv Sports. Evolv Adaptive Foot.
- [9] Mountain Orthotic & Prosthetic Services. ADK Rock Climbing Foot.
- [10] Kai Lin. KLIPPA: Prosthetic Leg for Rock Climbers.
- [11] Rino Versluys, Pieter Beyl, Michael Van Damme, Anja Desomer, Ronald Van Ham, and Dirk Lefeber. Prosthetic feet: state-of-the-art review and the importance of mimicking human ankle-foot biomechanics. *Disability and Rehabilitation. Assistive Technology*, 4(2):65–75, March 2009.
- [12] Merkur Alimusaj, Laetitia Fradet, Frank Braatz, Hans J. Gerner, and Sebastian I. Wolf. Kinematics and kinetics with an adaptive ankle foot system during stair ambulation of transtibial amputees. *Gait & Posture*, 30(3):356–363, October 2009.
- [13] Ossur. Proprio Foot.

- [14] Wayne Koniuk. Self-adjusting prosthetic ankle apparatus, September 2002.
- [15] Ryan J. Williams, Andrew H. Hansen, and Steven A. Gard. Prosthetic Ankle-Foot Mechanism Capable of Automatic Adaptation to the Walking Surface. *Journal of Biomechanical Engineering*, 131(3):035002–035002–7, January 2009.
- [16] Tommaso Lenzi, Marco Cempini, Jeremy Newkirk, Levi J. Hargrove, and Todd A. Kuiken. A lightweight robotic ankle prosthesis with non-backdrivable cam-based transmission. *IEEE ... International Conference on Rehabilitation Robotics: [proceedings]*, 2017:1142–1147, 2017.
- [17] Ottobock. Empower.
- [18] Tyler R. Clites, Matthew J. Carty, Jessica B. Ullauri, Matthew E. Carney, Luke M. Mooney, Jean-François Duval, Shriya S. Srinivasan, and Hugh M. Herr. Proprioception from a neurally controlled lower-extremity prosthesis. *Science Translational Medicine*, 10(443):1–13, May 2018.
- [19] Jean-Francois Duval and Hugh M. Herr. FlexSEA: Flexible, Scalable Electronics Architecture for wearable robotic applications. In *2016 6th IEEE International Conference on Biomedical Robotics and Biomechatronics (BioRob)*, pages 1236–1241, Singapore, Singapore, June 2016. IEEE.
- [20] Khalifa Harib and Krishnaswamy Srinivasan. Kinematic and dynamic analysis of Stewart platform-based machine tool structures. *Robotica*, 21:541–554, September 2003.
- [21] David A. Winter. *Biomechanics and Motor Control of Human Movement*. John Wiley & Sons, October 2009. Google-Books-ID: \_bFHL08IWfwC.
- [22] Claire L. Brockett and Graham J. Chapman. Biomechanics of the ankle. *Orthopaedics and Trauma*, 30(3):232–238, June 2016.
- [23] Paul Klein, Stephan Mattys, and Marcel Rooze. Moment arm length variations of selected muscles acting on talocrural and subtalar joints during movement: An In vitro study. *Journal of Biomechanics*, 29(1):21–30, January 1996.